Magnetoplumbite Nanostructures: Facile Synthesis, Structural and Transport Properties

By

Sana Mehmood

CIIT/FA13-PPH-009/ISB

PhD Thesis

In

Physics

COMSATS University Islamabad

Islamabad Campus-Pakistan

Spring, 2020

COMSATS University Islamabad

Magnetoplumbite Nanostructures: Facile Synthesis, Structural and Transport Properties

A Thesis Presented to

COMSATS University Islamabad, Islamabad

In partial fulfillment

of the requirement for the degree of

PhD Physics

By

Sana Mehmood

CIIT/FA13-PPH-009/ISB

Spring, 2020

Magnetoplumbite Nanostructures: Facile Synthesis, Structural and Transport Properties

A Post Graduate Thesis submitted to the Department of Physics as partial fulfillment of the requirement for the award of Degree of PhD in Physics.

Name	Registration Number
Sana Mehmood	CIIT/FA13-PPH-009/ISB

Supervisor

Prof. Dr. Muhammad Anis-ur-Rehman

Department of Physics

COMSATS University Islamabad (CUI), Islamabad

Certificate of Approval

This is to certify that the research work presented in this thesis, entitled "Magnetoplumbite Nanostructures: Facile Synthesis, Structural and Transport Properties" was conducted by Ms. Sana Mehmood, CIIT/FA13-PPH-009/ISB, under the supervision of Prof. Dr. Muhammad Anis-ur-Rehman, No part of this thesis has been submitted anywhere else for any other degree. This thesis is submitted to the Department of Physics, COMSATS University Islamabad, in the partial fulfillment of the requirement for the degree of Doctor of Philosophy in the field of Physics.

Student Name: Sana Mehmood Signature: _____

Examinations Committee:

Signature: _____
External Examiner 1:
Dr. Muhammad Maqsood
Director/Head Academics
NINVAST, NCP Complex, Islamabad.

Signature: _____
External Examiner 2:
Dr. M. Muneeb Asim
Deputy Director, NS & TD
NCP Complex, Islamabad.

Signature: _____
Prof. Dr. M. Anis-ur-Rehman
Supervisor
Department of Physics
CUI, Islamabad.

Signature: _____
Prof. Dr. Waqas Masood
HoD
Department of Physics
CUI, Islamabad.

Signature: _____
Prof. Dr. M. Anis-ur-Rehman
Chairman, Department of Physics
CUI, Islamabad.

Signature: _____
Prof. Dr. Aftab Khan
Dean, Faculty of Science
CUI, Islamabad.

Author's Declaration

I Sana Mehmood, CIIT/FA13-PPH-009/ISB, hereby state that my PhD thesis titled "Magnetoplumbite Nanostructures: Facile Synthesis, Structural and Transport Properties" is my own work and has not been submitted previously by me for taking any degree from this University i.e. COMSATS University Islamabad or anywhere else in the country/world.

At any time if my statement is found to be incorrect even after I graduate the University has the right to withdraw my PhD degree.

Date: _____

Signature of the student

Sana Mehmood

CIIT/FA13-PPH-009/ISB

The Art of writing only for samples use

Plagiarism Undertaking

I solemnly declare that research work presented in the thesis titled "Magnetoplumbite Nanostructures: Facile Synthesis, Structural and Transport Properties" is solely my research work with no significant contribution from any other person. Small contribution/help wherever taken has been duly acknowledged and that complete thesis has been written by me.

I understand the zero-tolerance policy of HEC and COMSATS University Islamabad towards plagiarism. Therefore, I as an author of the above titled thesis declare that no portion of my thesis has been plagiarized and any material used as reference is properly referred/cited.

I undertake if I am found guilty of any formal plagiarism in the above titled thesis even after award of PhD Degree, the University reserves the right to withdraw/revoke my PhD degree and that HEC and the university has the right to publish my name on the HEC/university website on which names of students are placed who submitted plagiarized thesis.

Date: _____

Signature of the student

Sana Mehmood

CIIT/FA13-PPH-009/ISB

The Art of writing only for samples use

Certificate

It is certified that Sana Mehmood, CIIT/FA13-PPH-009/ISB has carried out all the work related to this thesis under my supervision at the Department of Physics, COMSATS University Islamabad and the work fulfills the requirement for award of PhD degree.

Date: _____

Supervisor:

Prof. Dr. Muhammad Anis-ur-Rehman

Department of Physics

COMSATS University Islamabad

Head of Department:

Prof. Dr. Waqas Masood

Department of Physics

COMSATS University Islamabad

The Art of writing only for samples use

DEDICATION

This thesis is dedicated

To

My cute and adorable Grandmother, my loving Parents, Brothers

My supportive Husband and my naughty

Kids

Arsal Moin & Hadia Moin

The Art of writing only for samples use

ACKNOWLEDGEMENTS

Thanks to **ALLAH Almighty** and all the love and respect for his last **Prophet Muhammad (PBUH)**, who enlighten mankind with the essence of faith in **ALLAH** and guided them the true path of life.

At first, I would like to express my sincere gratitude to my supervisor **Prof. Dr. M. Anis-ur-Rehman** for extending great support, facilitation and guidance during days & nights, inside & outside lab. Under his leadership, motivation, and immense knowledge of the field, made it possible to complete my PhD research work successfully. I have no words to thank him. May **ALLAH (SWT)** bless him sound health and happiness always.

I would like to thank my lab fellows Dr. **Tanveer Akhtar**, Mr. **Yasir Abbas**, Mr. **Muhammad Kamran**, Mr. **Muhammad Tahir**, Mr. **Rizwan Khalid**, Mr. **Moiz ur-Rehman**, Mr. **Muhammad Khizar Javed (L)**, Mr. **Arsalan Munir,** Mr. **Rafique ur-Rehman**, Mr. **Shahid Rasheed**, Ms **Fatima-tuz-Zahra**, Ms **Sammar Tayyab**, Ms **Tasmiya Khalid**, Ms **Roohi Zahra**, Ms. **Faiza Arif**, Ms. **Uzma Afsar**, and Ms. **Nihal Niazi** for their technical- moral support and useful suggestions during my research work. I would also like to thank my friend Ms **Sehrish Azam** for her all time support and encouragement during study and research work.

I would like to thank all faculty members and especially **Dr. Zahid Imran** and **Dr. Hamza Qayyum** for their kind support and valuable suggestions. Especial thanks to **Chairperson Department of Physics** and **Dean Faculty of Sciences**, for their cooperation. I am also thankful to **all staff members** and especially Mr. **Amjad Kalyar** for academic coordination and kind facilitation. Support of **Dr. Guiliana Aquilanti**, **Dr. Luca Olivei**, **Dr. Andrea Cognigni** is greatfully acknowledged for XAFS beamline and collection of data at ELETTRA Synchrotron, Trieste, Italy through ICTP-ELETTRA Users' Programme. I express my heartful thanks to Mrs. **Uzma Alamdar** for her unconditional support and prayers. I am thankful to my darling **Mom and Dad**, my loving **Brothers**, my supportive **Husband**, lovely **Kids**, and **In-laws** for their all times prayers, encouragements and moral support.

Sana Mehmood

CIIT/FA13-PPH-009/ISB

Abstract

Magnetoplumbite Nanostructures:
Facile Synthesis, Structural and Transport Properties

Magnetoplumbite-type ferrites (M-type hexaferrites) have a wide range of applications. These have been extensively studied due to their interesting properties. These are found in or used to produce almost every modern convenience today. In the present work, we have synthesized undoped and divalent & trivalent doped strontium hexaferrites. The samples series made were $SrFe_{12}O_{19}$, $SrFe_{12-2x}A_xB_xO_{19}$ and $SrFe_{12-x}B_xO_{19}$, where (A =Zn, B=Cr and x= 0.0, 0.2, 0.4, 0.6, 0.8, 1.0). Doping was made at octahedral Iron (B) site with a suitable proportion through wet-chemical methods. The prepared samples have applications in high frequency devices. Their magnetic properties are usually investigated and are available in the literature but their transport properties (electrical and thermal transport) with respect to frequency and temperature and especially their correlation with structural changes is very rare. The knowledge and understanding of the correlation between those are of crucial importance for the development of the materials with desirable properties.

For structural and morphology characterization, X-ray diffraction (XRD), Fourier Transform Infrared Spectroscopy (FTIR), X-ray Absorption Near Edge Structure (XANES) spectroscopy, Extended X-ray Absorption Fine Structure (EXAFS) Analysis and Scanning Electron Microscopy (SEM) have been carried out for the selected compositions. AC electrical properties as a function of frequency (1 kHz to 3-MHz) and in temperature range (100ºC to 300ºC) were also studied. At the fixed frequency of 500 kHz and 1-MHz, electrical properties of the prepared sample materials were also investigated. DC electrical properties as a function of temperature (100-500ºC) have also been measured. Impedance analysis has been done to understand the grain and grain boundary effects. Thermal properties of materials like volumetric heat capacity, thermal conductivity and the thermal diffusivity have been performed by using Advantageous Transient Plane Source (ATPS) method. The variations of dielectric constant and dielectric loss have been explained based on Maxwell-Wagner models. Finally, the correlation of results has been performed to investigate the structural changes with electrical and the thermal transport properties of the synthesized materials.

In the first part, Magnetoplumbite-type, $SrFe_{12}O_{19}$ hexaferrite samples were synthesized by using two wet chemical methods i.e., sol-gel and co-precipitation method. Structural and electrical properties with respect to frequency and temperature

The Art of writing only for samples use

were investigated. XRD pattern showed hexagonal structure with traces of αFe_2O_3 phase. However, for the samples prepared by co-precipitation method showed higher intensity of αFe_2O_3 phase. Lattice constants 'a' and 'c' are nearly same with in the error range. FTIR analysis confirmed the formation of magnetoplumbite structure. SEM images showed agglomeration of particles. The maximum intensity peak crystallite size was found to be 67nm for both the samples. At the frequency of 1kHz and temperature 300ºC, the dielectric constant for sol-gel synthesized sample have value 29.51 whereas samples synthesized by co-precipitation method have value 21.13. For the same frequency and temperature, tangent loss for samples synthesized by sol-gel and co-precipitation method was found to be 0.30 and 5.28 respectively. Impedance analysis revealed that at a fixed frequency of 500kHz and temperature of 100ºC the sol-gel prepared material has higher value that is 126 kOhm whereas for co-precipitation prepared sample it was 60 kOhm. The phase transformation was observed in the temperature range of 400ºC to500ºC. Bulk effect was observed in Cole-Cole plots. DC resistivity for sol-gel and co-precipitate synthesized materials at the temperature of 200ºC was found to be 28 MOhm-m and 3MOhm-m respectively.

Transition metal doped strontium hexaferrites have shown improved dielectric properties. Cr and Zn were selected for this improvement. In the second and third phase of our work, we prepared samples of $SrFe_{12-2x}Cr_xZ_xO_{19}$ (x=0.0, 0.2, 0.4, 0.6, 0.8, 1.0) by co-precipitation and sol-gel methods respectively. Lattice parameters obtained from XRD data showed non monotonous behavior with respect to composition. Stresses and strains were observed and were determined in the samples, made by both techniques. Sol-gel prepared samples showed tensile strain whereas co-precipitated sample with composition x=1.0 showed compressional strain. XAFS analysis was performed for local atomic structural investigations of Cr-Zn doped $SrFe_{12-2x}Cr_xZ_xO_{19}$ (x=0.0, 0.2, 0.4, 0.6, 0.8, 1.0) samples, prepared by sol-gel technique. Valence state, cationic-distribution, interstitial sites occupancy and atomic bond-length in the pure Magnetoplumbite and Cr-Zn doped sample compositions were studied. Dielectric properties as function of frequency and temperature were also studied. At a frequency of 1kHz and temperature of 300ºC the sol-gel prepared composition x=0.2 showed high value of dielectric constant 426.57 at the same frequency and temperature co-precipitate sample composition x=1.0 showed dielectric constant value 26.60. Jonscher's Power Law revealed that value of 'n' decreased with the increase of temperature. CBH (Correlated Barrier Hopping) mechanism was suggested for both the prepared samples. The impedance analysis at a fixed frequency of 500 kHz and

The Art of writing only for samples use

temperature of 100ºC showed that the composition x= 0.0 prepared by sol-gel method had high value of impedance 126 kOhm whereas at the same temperature and frequency co-precipitate sample with composition x=0.6 have impedance value 93 kOhm. Temperature dependent dielectric constant at two fixed frequencies for the composition x=0.2 prepared by sol-gel method showed a wide gap. This composition can be used as a ferroelectric relaxor. Phase transformation from ferroelectric to paraelectric, for both the prepared samples were in the range of 400ºC to 500ºC. Cole-Cole plots were also drawn to understand the grain and grain boundary effect. Maximum dc resistivity for sol-gel prepared composition x=0.4 have value 154 kOhm-m whereas sample prepared by co-precipitation method with composition x=0.2 have value 5 MOhm-m.

In the fourth phase of the work, single dopant Cr was selected for in-depth local structure and conduction correlation studies. The compositions $SrFe_{12-x}Cr_xO_{19}$ (where x= 0.0, 0.2, 0.4, 0.6, 0.8, 1.0) were synthesized by using sol-gel method since from previous comparison, we came to know sol-gel gives good results as compared to that of co-precipitation method. In literature, it is reported that Cr^{3+} after certain composition starts behaving surprisingly. So, to understand the behavior of this material, we studied the structural electrical and the thermal properties of this material. Structural analysis was done by XRD, FTIR, XANES and EXAFS. XRD revealed the formation of hexagonal structure. All bands in FTIR spectra were in the fingerprint region of Strontium hexaferrite. XANES and EXAFS analysis helped to investigate the absorption energy, chemical environment of the absorbing atom, their oxidation state and the bond lengths. For x=0.0 and x=0.2, Cr^{3+} had octahedral site occupancy however it was observed that after x=0.4 composition, Cr^{3+} occupied tetrahedral site, which resulted in non-monotonous conduction properties. Dielectric properties as a function of frequency and temperature were also studied. Composition x=0.2 was found to have the highest value of dielectric constant 79.45. Cole-Cole plots showed the presence of bulk effect in the system. At room temperature thermal analysis has been done. The conductivity of the material showed nonlinear behavior as due to stress and strains the hexaferrite lattice simply deformed. These variable properties have made them suitable for various applications like speakers in mobile phones to the electric motors in hybrid cars, transducers, electric bicycles, wind power generators, energy generators or storage devices, microwave fields, magnetic storage discs, magnetic separation, magnetic shielding and in many high frequency devices.

Table of Contents

The Art of writing only for samples use

The Art of writing only for samples use

The Art of writing only for samples use

The Art of writing only for samples use

List of figures

The Art of writing only for samples use

The Art of writing only for samples use

The Art of writing only for samples use

The Art of writing only for samples use

The Art of writing only for samples use

List of Tables

LIST OF ABBREVIATIONS

$D_{max\text{-}int}$	Crystallite size of peak with maximum intensity
ΔE	Activation energy
έ	Dielectric constant
ε_0	Permittivity of free space
ρ_x	X-ray density
ρ_{dc}	DC electrical resistivity
Sr-Hexaferrite	Strontium hexaferrite
XRD	X-Ray diffraction
FTIR	Fourier Transform Infrared Spectroscopy
σ_{AC}	AC conductivity
tan δ	Dielectric loss tangent
SEM	Scanning Electron Microscope
XAFS	X-ray Absorption Fine Structure
XANES	X-ray Absorption Near Edge Spectroscopy
EXAFS	Extended X-ray Absorption Fine Spectroscopy
CN	Coordination Number
Z	Impedance
Z′	Real part of Impedance
Z″	Imaginary part of Impedance

The Art of writing only for samples use

List of Publications

1) Sana Mehmood, & M. Anis-ur-Rehman, Correlation of structural and electrical properties in heterovalent substituted Sr-hexaferrites, Mater. Res. Express, 6 (12), 126328, 2020. DOI: 10.1088/2053-1591/ab6644.

2) Sana Mehmood & M. Anis-ur-Rehman, Association of Structural Strains and Dielectric relaxation in Co-doped Sr-Hexaferrites, Physica B: Condensed Matter, 582, 412003, 2020. DOI:10.1016/j.physb.2020.412003

3) Sana Mehmood, M.F. Natiq & M. Anis-ur-Rehman, X-rays Absorption Spectroscopy for local structure determination of Magnetoplumbite nanoparticles, J. Alloys. Comp, 869, 159355, 2021. DOI: 10.1016/j.jallcom.2021.159350

The Art of writing only for samples use

International Conference Presentation

1) "Influence of temperature on structural and electrical properties of Cr-Zn substituted M type strontium hexaferrite Nanomaterials" in 16th International Symposium on Advanced materials (ISAM) 2019 from 21st to 25th October at National Centre for Physics Islamabad, Pakistan.
2) "Temperature Dependent Structural and Electrical Properties of Cr-Zn substituted M-Type Strontium Hexaferrite Nanomaterials" International Conference on Superconductivity and Magnetism, (ICSM) from 28th April to 4th May 2018, held in Turkey.
3) "Variation in the structural and the electrical properties of Cr-Zn doped Strontium hexaferrites" in 15th International Symposium on Advanced materials (ISAM) 2017 from 16th to 20th October at National Centre for Physics Islamabad, Pakistan.
4) "Effect of Varying Sintering Temperature on Electrical Properties of Mn-Zn ferrites" First International Conference on Mathematics and Physics 2017 from 12th to 16th February at Air University Islamabad, Pakistan.
5) "Effect of Sintering on the Structural and Electrical Properties of Co-precipitated Mn-Zn Nano ferrites" 14th International Symposium on Advanced Materials (ISAM) 2015 from 12th to 16th October at National Centre of Physics Islamabad, Pakistan.
6) "Conduction in co-precipitated Mn-Zn Nanoferrites" International Conference on Physics and contemporary Needs, 19th to 21st November 2014 at GCU Lahore, Pakistan.

The Art of writing only for samples use

Chapter 1

Introduction

1.1 Materials at Nano scale

Material at Nano scale or nano materials are those materials which have at least one dimension in nano meter scale. These materials usually differ in properties from the bulk materials due to quantum and surface effects. The features like particle size, shape, grains do play major role in describing the electronic and functional properties. These properties are associated with the variations produced in lattice structural parameters, type and concentration of dopant and the method by which these materials are synthesized [1]. From the last 20 years, nanotechnology has enabled scientists to build nano materials with controlled structures to utilize the naturally occurring physical, chemical, electrical, mechanical, optical and magnetic properties for efforts to significantly improve industrial and technological sectors. These include information technology for electronics and IT applications, medicine for medical and health care applications, transportation, energy/power generation, food safety and environmental science among others [2].

1.2 The World of Ferrites

Ferrites can be defined as the ferromagnetic oxide types of materials, which possess high resistivity and permeability [3]. Ferrites contain Fe^{3+} ions as the major cation and have advantages over other magnetic materials due to their applications in high frequency devices, higher resistivity, heat resistance, corrosion resistance and low price. Commercial applications of ferrites started by 1950 in the electronic communication industry like Radio, TV, telephone, and computer circuits and micro waves machines [2]. Later on ferrites got great success in applications for power generation, information storage, permanent magnets and in motors for industrial applications. Depending upon the application, the electrical, magnetic and other properties of ferrites can be adjusted with many techniques like synthesis conditions, sintering and calcination temperatures, type and amount of dopants and synthesis method. The canvas of ferrites applications got bigger with the advent of nano scale ferrites particles. Nano ferrites with size less than 20 nm got applications for devices useful for data storage devices, energy sector, biomedical sector for treatment of cancer and other diseases [4]. In recent times, ferrites have got numerous applications in transducers, antennas for communications, memory storage devices etc.

The Art of writing only for samples use

1.3 Different Kinds of Ferrites

Ferrites can be divided into two unique groups or streams, one based on the crystal structure, referred to as cubic and hexagonal ferrites and other based on magnetic features, referred to as soft and hard ferrites [5]. According to crystal structure, these materials are classified into Spinel, Garnet, Hexagonal and Orthoferrites. Spinel and Garnet ferrites do possess cubic crystal structure whereas Hexaferrites possess magnetoplumbite nature of structure. While, Orthoferrites have perovskite type structure [6-7].

Table1.1: Classification of ferrites

Ferrites	Crystal Structure	Composition
Spinel	Cubic	$\boldsymbol{M^{2+}Fe_2^{3+}O_4}$ I= Mn^{2+}, Ni^{2+}, Zn^{2+}, Mg^{2+}, Cu^{2+} ions or their combination
Garnet	Cubic	$\boldsymbol{R^{3+}Fe_5^{3+}O_{12}}$ R= Y^{3+}, Gd^{3+}
Hexaferrite	Magnetoplumbite or Hexagonal	$\boldsymbol{M^{2+}Fe_{12}^{3+}O_{19}}$
Orthoferrite	Orthorhombic Perovskite	$\boldsymbol{R^{3+}Fe^{3+}O_3}$ R^{3+} = Y^{3+}, Gd^{3+}, Nd^{3+}, Sm^{3+}, Lu^{3+}

1.3.1 Spinel Ferrites

Spinel ferrites have general formula $M^{2+}Fe_2^{3+}O_4$, (M = Metal cation like Mn^{2+}, Ni^{2+}, Zn^{2+}, Cd^{2+}, Fe^{2+} etc.). These materials have high D.C resistivity and good magnetic properties [8].

Spinel ferrites have applications in devices operable at in Mega Hertz frequencies.

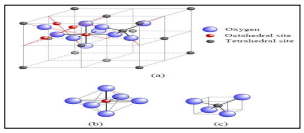

Fig 1.1(a): Spinel unit cell structure, (b) octahedral interstice (B) site (c) tetrahedral interstice (A) site [6-7]

The Art of writing only for samples use

1.3.2 Garnet Ferrites

Garnet ferrites are represented by a formula $M_3(Fe_5O_{12})$. Here, M can be referred to as a Yttrium or Rare-Earth ion. They have cubic structure and are regarded as hard magnetic materials.

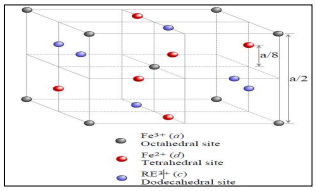

Fig 1.2: Garnet crystal structure, a represent lattice constant [6,7]

1.3.3 Magnetoplumbite or Hexagonal Ferrites

Hexaferrites are regarded as one of the most attractive ferrites materials which are famous for their industrial and technological applications. They are generally represented with chemical formula $M^{2+}Fe_{12}^{3+}O_{19}$. Where (M = Sr^{2+}, Pb^{2+}, Ba^{2+}, Pb^{2+} or Ca^{2+} etc). The major beauty of Magnetoplumbite structure is that the required properties of the materials can be tuned or upgraded for a specific need as per applications. The famous Strontium hexaferrites belong to hexagonal ferrites. These are one of the best choice for applications in higher frequency devices, telecommunication devices and as permanent magnets due to many reasons like higher electric resistance, chemically and thermally stable from -40ºC to 200ºC, low corrosion, low cost and environment friendly, high values of coercivity, high chemical stability and uniaxial anisotropy [9]. The crystal structure of hexaferrites is composed of layers of tightly packed large anions as Oxygen or Cations as (Sr^{2+}, Pb^{2+}, Ba^{2+}, Pb^{2+} or Ca^{2+} etc.). The interstitial cavities or sites are occupied by Fe^{3+} or Fe^{2+} ions. Other elements with divalent or trivalent ion (Zn^{2+}, Ni^{2+}, Al^{3+}, Ti^{4+} etc.) can also be introduced. The unit cell of hexagonal ferrites is considered to be composed of repeated units of three smaller blocks like S, R and T. The orientation and stacking of these blocks along hexagonal

The Art of writing only for samples use

axis can be modified in many ways, leading towards development of a various other hexagonal ferrites [10-12].

1.4 Structural blocks in hexagonal ferrites

The block S,R and T are composed of two, three and four in nmber of oxygen layers havig small cations as interstitial sites respectively. Large cations are also located in the inner structure of blocks S and T. Small cations are commonly shared between two neighbouring blocks. The structral blocks are shown in figure 1.3. Based on these basic blocks, hexagonal ferrites can be further classified into following catagories, described in table 1.2 [13].

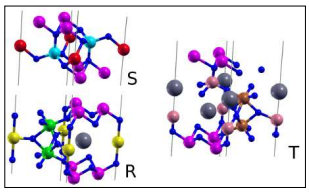

Fig 1.3: Structural blocks in hexagonal ferrites [6-7]

Table 1.2 Classification of hexaferrites

Symbol	Chemical Formula	Unit cell Structure	No of oxygen layers
M	$BaFe_{12}O_{19}$	RSR*S*	10
W (M+S)	$BaMe_2Fe_{16}O_{27}$	RSSR*S*S*	14
Y	$Ba_2Me_2Fe_{12}O_{22}$	3 (ST)	18
Z (M+Y)	$Ba_3Me_2Fe_{24}O_{41}$	RSTSR*S*T*S*	22
X (2M+S)	$Ba_2Me_2Fe_{28}O_{46}$	3(RSR*S*S*)	36
U (2M+Y)	$Ba_4Me_{12}Fe_{36}O_{60}$	RSR*S*T*S*	16

1.5 M Type Hexagonal Ferrites

Magnetoplumbite or shortly M-type hexaferrites have regular repeating R and S blocks in their structure such that in its one-unit cell, RSR*S* blocks are present. Where *

describes the rotation of that particular block at an angle of 180°, around hexagonal c axis. These M type ferrites or Magnetoplumbite are expressed with general chemical formula $MFe_{12}O_{19}$. Also, a single unit cell of $MFe_{12}O_{19}$ posses two formula units and contains $P6_3/mmc$ space group. The cations M^{2+} and Fe^{3+} occupy sites among the oxygen lattice in M type hexagonal ferrites. There are 38 Oxygen ions, 24 Iron and 2 M type divalent ions per unit cell. The M^{2+} cations reside at 2d sites [14] whereas Iron ions settle themselve among five distinct iterstitial crystallographic sites. Among those site, there exist three octahedral sites, one tetrahedral and one bipyramidal site [15]. The lattice constant values are c ≈ 23.2 Å and a=b ≈ 5.86 Å with 1% of variation in $BaFe_{12}O_{19}$, $SrFe_{12}O_{19}$ and $PbFe_{12}O_{19}$ systems [16-17].

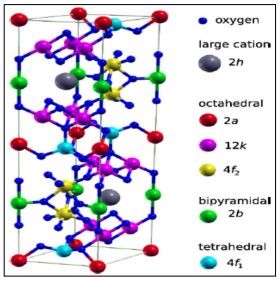

Fig 1.4: Unit cell of M type hexagonal ferrite [6-7]

1.5.1 Strontium Hexagonal Ferrites

Strontium ferrites ($SrFe_{12}O_{19}$) has uniaxial Magnetoplumbite structure (space group P63/mmc), with excellent magnetization anisotropic nature, well chemical stability and high coercivity feature. Discovered in the 20th century, Strontium hexaferrites are one of the most studied magnetic materials because of their commercial importance like its high electric resistance, non-toxic nature, corrosion resistance, chemical and thermal durability and low electric losses [18]. These materials have numerous applications both in industry and high-tech fields like permanent magnets, data storage devices, high frequency devices used in telecommunication and radar [19-20]. $SrFe_{12}O_{19}$ is ferrimagnetic in nature. Its curie temperature is around 723K and magnetic moment

about 17μB to 21 μB per formula unit [21]. $SrFe_{12}O_{19}$ crystal structure is shown in figure 1.5 which can be regarded as a layered structures of S (Spinel) and R (Rock salt) blocks stacked over one another in such a way that Sr^{2+} ions reside in R-block. The crystallographic structure built on block formation as RSR*S* are described by Braun [22]. In Magnetoplumbite crystal structure, block S is of cubic nature and R block contains hexagonal structure. There are 24 Iron atoms in it, all of which have Fe^{3+} oxidation state and reside in five distinct sites 2a, 2b, $4f_1$, $4f_2$, and 12k which is as per Wickhoff's notation [23]. The 24 iron (Fe^{3+}) ions dispersed among three octahedral (B) sites, one tetrahedral (A) site and one trigonal bipyramid shaped site which is bounded by five in numbers oxygen atoms. Magnetic properties like magnetic moment and magneto-crystalline anisotropy are also influenced by Fe^{3+} ionic structure, located at five different magnetic sub-lattices [24-25]. Further, the physical, electric, dielectric properties depend on the chemical environment, distribution of cations and the method by which they are synthesized [26].

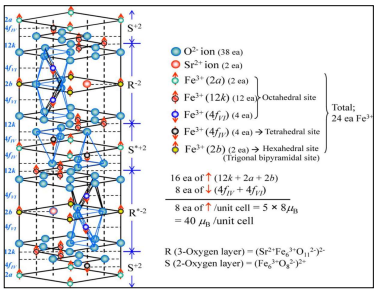

Fig 1.5: Crystal Structure of Strontium hexaferrites [26]

1.6 Applications of Hexagonal Ferrites

According to a latest magnet market report [27], ferrites business share in the world's magnet market might touch US$ 7.11 billion by the year 2024. The report also highlighted that in 2018, the ferrites magnets market reached upto US$ 5.68 billion worldwide. In today's world, magnets have been used in many ways for numerous applications for example, in mobiles, transformers, transport vehicles, communication

devices, generators & motors, actuators & sensors, devices for information storage, food safety and security, defense items, aviation industry, medical field for diagnostic of diseases and medication. Hexagonal ferrites are very demanding and commercially used materials due to many reasons. First and the foremost reason is that these materials are the most economical to manufacture than the other types of ferrites. They are less toxic and as for as magnetic properties are concerned they have much superior properties than the rest of the ferrite materials because they are hard and resist against demagnetization. Some of the major applications of hexagonal ferrites are shown in figure 1.6 below

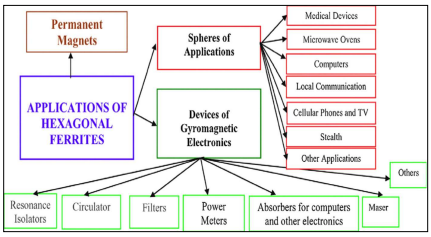

Fig 1.6: Different Applications of hexaferrites [23]

Rare Earth (RE) metal and alloys magnets are considered to be the best permanent magnets however due to scarcity of Rare earth metals in the world; these RE based magnets are very expensive. The researchers have looked for the alternative materials for magnet applications. Among hexagonal ferrites, Strontium and Barium based hexaferrites are far superior to others in applications for permanent magnets. Presently, hard ferrites magnets have been used in many ways for numerous applications for examples in electro-acoustic devices, Bluetooth, loudspeakers, microphones, intercom sets, mobiles, transformers, modern transport vehicles braking and locking system, communicating helmets, 5G/6G communication technology devices , generators & motors, actuators & sensors, devices for information storage, food safety and security, defense items, aviation industry, medical field for diagnostic of disease and medication [23].

1.7 Literature Review

The ferrites properties can be tailored by modifying the crystal structure, the composition, synthesis method, synthesis conditions, cationic-distribution, type and concentration of dopant used [28]. Intensive work has been done to modify the structural, electrical, and magnetic properties of strontium hexaferrites by substitution of Fe^{3+} ions with other combination of cations, changing synthesis route or varying the concentration of used dopants [29]. During studies on introduction of transition metal cation like Co^{2+}, Ti^{4+}, Ir^{4+}, Zn^{2+} and Mn^{2+} etc. and replacement of Fe^{3+} ions in magnetoplumbite structures coercivity was observed to be reduced. However, the magnetization of doped particles was also found to be decreased [30-32]. It limits hexaferrite applications for magnetic recordings applications. So, the big challenge was attaining decrease in coercivity and increase saturation magnetization parameters together. This challenge attracted great attentions of researchers all over the world and many efforts were made to address the issue. Q.Q. Fang, et.al (2005) found that increase in saturation magnetization and lower coercivity combination is possible with Cr^{3+} doping in $SrFe_{12}O_{19}$ with optimal doping concentration $x \leq 0.4$ however, a non-magnetic phase could also observed [31].

Y. Slimani, et.al (2018) had developed chromium doped Nano-hexaferrites series $SrCr_xFe_{12-x}O_{19}$ ($0.0 \leq x \leq 1.0$) using hydrothermal technique. Upon comparing the results with the bulk $SrFe_{12}O_{19}$ the magnetic properties were observed to be increase for Cr^{3+} concentration ($x \leq 0.4$). After that a decrease was observed upon increasing of Cr^{3+} contents [33]. E. Roohani, et.al (2018) prepared samples of $SrFe_{12-x}Cr_xO_{19}$ series (x = 0, 0.25, 0.5, 0.75, 1) and analyzed earlier, the coercively of material samples is decreased and then increases upon adding more chromium contents in system. However, saturation magnetization first increases with chromium contents addition up to (x = 0.25) and then starts decreasing for higher concentration of Cr^{3+} dopants [34].

Z. Wu, et.al (2018) studied Gd-Cu doping effects in M type hexaferrites with nominal composition $Sr_{1-x}Gd_xFe_{12-x}Cu_xO_{19}$ ($x = 0.00, 0.05, 0.10, 0.15$ and 0.20) prepared by solid phase method. Preparation and magnetic behaviors were investigated [35]. M. Alimoradi, et.al (2019) studied Al^{3+}/Cr^{3+} doping effects in M type Barium hexagonal ferrites $BaAl_xCr_yFe_{11}O_{19}$ ($x + y = 1$) synthesized using sol-gel method. It

was found that with Al^{3+}/Cr^{3+} increased concentration, the remanent, saturation magnetization are reduced whereas the coercivity is improved from 5215 Oe to 7178 Oe [36]. S.N. Kamde, et.al (2019) prepared Cr^{3+} doped $SrFe_{12-x}Cr_xO_{19}$ hexaferrite nano crystalline particles using sol-gel method. On studying electrical and magnetic behaviors, it was observed that magnetic parameters were found to be different from bulk values [37]. M. Tasleem, et.al (2019) investigated Copper and Cobalt doping effects in the nano $SrBaFe_{12}O_{19}$, series with nominal composition $Sr_{0.5}Ba_{0.5}Fe_{12-2x}Co_xCu_xO_{19}$ ($x = 0.0$-0.8) developed using sol-gel method. Optical and electronic properties were investigated [38].

D. Makovec, et.al (2019) studied Sc^{3+} doping effects in the structure of barium-hexaferrite nano platelets in comparison with bulk. Magnetic behavior in nano platelets was opposite to that, obtained in the bulk [39]. D.A. Vinnik et.al (2019) developed single crystal of M type $SrFe_{12}O_{19}$ of size 5 mm by spontaneous crystallization method. The single crystal behaved as ideal soft ferrite with respect to magnetic properties [40]. M.A. Almessiere, et.al (2019) studied Manganese (Mn) and Yttrium (Y) doped Strontium nano hexaferrites with nominal composition $Sr_{1-x}Mn_xFe_{12-y}Y_yO_{19}$, where $0.0 \leq x = y \leq 0.5$), synthesized with sol-gel auto combustion method. The magnetic parameters were observed to be decreased upon increasing the dopants Mn^{2+} and Y^{3+} contents [41].

A. Liaquat, et.al (2020) prepared Rare-Earth element Gd^{3+} doped Sr-Ba $Fe_{12}O_{19}$ nanoparticles by WOWS sol-gel method and investigated impact on dielectric and magnetic properties [42]. T.L. Phan, et.al (2019) studied hexagonal $BaCo_{1-x}Mn_xFe_{11}O_{19}$ (x=0.0-1.0), synthesized by co-precipitation method and investigated the crystalline electronic structure along with magnetic properties. The cation did not show any change in their oxidation state [43]. G.D. Soria, et.al (2019) synthesized Strontium hexaferrite ($SrFe_{12}O_{19}$) platelets of size, micrometers in width and tens of nanometers in thickness using hydrothermal method. Structural analysis was performed using Mössbauer spectroscopy and soft X-ray absorption techniques. The absorption of Iron Fe L edge and Oxygen-K edge were measured [44].

N. Tran, et.al (2018) studied $Ba_{1-x}Sr_xCoFe_{11}O_{19}$ hexaferrites nanoparticles, synthesized by precipitation method. The oxidation states Fe^{3+} and Co^{2+} in the material were determined and magnetic properties were correlated [45]. N. Tran, et.al (2019)

also studied Co doped compositions $BaFe_{12-x}Co_xO_{19}$ (x= 0-2), by XRD and XAFS techniques. XRD technique suggested distortion in the lattice with Co doping at Fe^{3+} sites with reduction in the permanent magnetic properties. Site occupancy was studied with XAFS technique [46]. S.N. Kamde, et.al (2019) studied magnetic, electrical, and structural properties of $SrFe_{12}O_{19}$ Hexaferrite. materials were studied. Materials were recommended for magnetic recording devices [47].

M. Anis-ur-Rehman (2019) for his research on energy efficient Magnetoplumbite nano-sized ferrites, prepared Strontium hexaferrites and Sr-Ba hexaferrites $Sr_{1-x}Ba_xFe_{12-y}Gd_yO_{19}$ series (x=0.0, 0.25, y=0.0, 0.20) by WOWS sol-gel and Co-precipitation methods. Structural, dielectric and electrical properties with temperature were studied. Increase in resistivity was observed [48]. D.A. Vinnik, et.al (2019) studied heavily doped Magnetoplumbite hexaferrites compositions of $Ba(Fe_6Ti_{1.2}Co_{1.2}In_{1.2}Ga_{1.2}Cr_{1.2})O_{19}$. Composition with maximum entropy having single phase was identified by element analysis. Suitable sintering temperature and dopant concentration were also reported [49].

D.A. Vinnik, et.al (2019) studied single crystals of Magnetoplumbite $SrFe_{12}O_{19}$ for structural and magnetic analysis. The crystals were recommended for soft magnetic application [50]. S.A. Mathews, et.al (2020) studied the magnetic behavior of $Ba_{0.5}Sr_{0.5}Fe_{12}O_{19}/NiFe_2O_4$ nano materials, prepared samples from updated sol-gel technique. Fabricated samples were suitable for microwave absorber applications [51].

1.8 Research Motivation and Objectives

After a thorough literature review, it was observed that electrical, magnetic, optical and structural properties of magnetoplumbite hexaferrite materials have been widely studied however, when these materials are used in actual devices, the losses are high which limit the suitability and performance of these materials. Therefore, enhancement of electrical resistivity, controlling dielectric properties and low losses are utmost requirements for these materials applications in high frequency devices. Transport properties (electrical and thermal transport) with respect to frequency and temperature and especially their correlation with structural changes is not available in literature, to the best of our knowledge. The knowledge and understanding of the correlation

between these are of crucial importance for the development of the materials with desirable properties.

In the present work, we have synthesized Magnetoplumbite samples series $SrFe_{12-2x}A_xB_xO_{19}$ and $SrFe_{12-x}B_xO_{19}$, by substituting divalent (A^{+2}), trivalent (B^{+3}) ions as dopants at octahedral Iron (B) site with a suitable proportion through wet-chemical methods. For Structural and Morphology characterization, X-ray Diffraction (XRD), X-rays Absorption Fine Spectroscopy (XANES and EXAFS), Fourier Transform Infrared Spectroscopy (FTIR) and Scanning Electron Microscopy (SEM) have been carried out for the prepared compositions. With the help of XAFS analysis local structure information is determined. Electrical properties as a function of frequency and temperature are also studied and correlated with the structural information. Impedance analysis has also been done to understand the grain and grain boundary effect. Thermal properties of materials like volumetric heat capacity, thermal conductivity and the thermal diffusivity have been performed by using Advantageous Transient Plane Source (ATPS) method. The variations of dielectric constant and dielectric loss have been explained based on Maxwell-Wagner models. Finally, the correlation of results has been performed to investigate the dependence of electrical and thermal transport properties on the structure of the synthesized materials. Prepared samples have wide range of applications.

1.9 Flow Chart of Work Plan

The detailed process flow chart for the research work plan is described in figure 1.7.

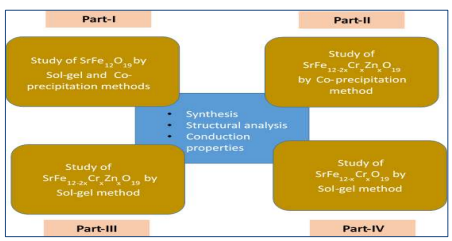

Fig 1.7: Process flow chart of research work plan

1.10 Thesis Synopsis

During the research work, samples of magnetoplumbite Strontium hexaferrites ($SrFe_{12}O_{19}$), Cr-Zn doped Strontium hexaferrite ($SrFe_{12-2x}Cr_xZ_xO_{19}$) with nominal composition (x=0.0, 0.2, 0.4, 0.6, 0.8, 1.0) were synthesized by Sol-gel and Co-precipitation methods. After that Cr doped Strontium hexaferrite ($SrFe_{12-x}CrO_{19}$) with nominal composition (x=0.0, 0.2, 0.4, 0.6, 0.8, 1.0) were synthesized by Sol-gel method. Then, Elettra-Sincrotrone Trieste, Italy was approached for XAFS beam line data collection and analysis to probe the local atomic structural investigations in depth. After that electrical and thermal transport properties were measured with respect to frequency and temperature and finally correlation with structural changes was carried out. In order to describe research work in dissertation, work is distributed into nine chapters. Chapter wise details are as follow.

In Chapter 1, introduction about the ferrites, their different types is given. Then structure of different types of hexagonal ferrites is discussed and especially Magnetoplumbite type Strontium hexaferrite structure is elaborated in detail. Applications of hexaferrites and comprehensive literature review are described in depth. In the end, research motivation is also mentioned

Chapter 2 is about synthesis techniques. In this chapter, we have described two different types of techniques (Top-down and bottom-up) for synthesis of Magnetoplumbite hexaferrites. Sol-gel and Co-precipitation methods which are used for samples preparation of during research, are also discussed in-length.

Chapter 3 is about characterizations techniques employed to characterize the samples during our research. The equipment used for Structural, Electrical and Thermal properties, their working principles, schematic diagrams and basics governing equations for characterizations of prepared samples are discussed in detail.

Chapter 4 is about understanding the structure and electrical properties of magnetoplumbite $SrFe_{12}O_{19}$ samples prepared by Sol-gel and co-precipitation methods. For Structural and morphology analysis, results from XRD, FTIR and SEM are given. For AC electrical properties with respect to frequency (1 kHz to 3-MHz) and temperature (100 ^oC to 300^oC), parameters like Dielectric constant, Dielectric tangent loss (tan δ), Conductivity, Impedance with Real and Imaginary parts and Cole-Cole

plots are discussed. AC electrical responses for same parameters have also been studied at two fixed frequencies (500 kHz and 1-MHz). DC Resistivity including activation energies of the prepared samples is also given using the Arrhenius relation. In the end, conclusion of results is also mentioned.

Chapter 5 is related to study of structural and electrical properties of (Cr-Zn) doped Strontium hexaferrites compositions $SrFe_{12-2x}Cr_xZn_xO_{19}$ series (x = 0.0 to 1.0) prepared by Co-precipitation method. XRD, FTIR and SEM results of prepared samples are provided for structural studies. AC electrical properties with respect to frequency (1 kHz-3-MHz) and temperature (100 °C to 300°C) for parameters like Dielectric constant, Dielectric tangent loss (tan δ), Conductivity, Impedance with Real and Imaginary parts and Cole-Cole plots are described. AC electrical responses at two fixed frequencies (500 kHz and 1-MHz) are also given for above mentioned parameters. DC electrical properties with change in temperature (100°C to 500°C) for prepared samples compositions are also discussed.

Chapter 6 deals with the Study of magnetoplumbite structural, electrical and thermal properties of $SrFe_{12-2x}Cr_xZn_xO_{19}$ (x = 0.0 to 1.0) prepared by Sol-gel method. It's one of the distinguish features are structural investigation by using XANES and EXAFS analysis techniques, in addition to XRD, FTIR and SEM analysis. AC Electrical properties with respect to, variable frequency (1-kHz to 3MHz) & Temperature (100 °C to 300°C), and two fixed frequencies 500 kHz and 1-MHz are also discussed for all parameters as mentioned in previous chapters. DC electrical properties with change in temperature (100°C to 500°C) are also discussed. In the end, thermal analysis of prepared samples is also appended.

Chapter 7 is study of Cr^{3+} doped magnetoplumbite structural, electrical and thermal properties of $SrFe_{12-x}Cr_xO_{19}$ (x = 0.0 to 1.0) prepared by Sol-gel method. For structural investigations XRD, FTIR, SEM, XANES and EXAFS analysis techniques are employed. AC Electrical properties are measured in same pattern as discussed in all previous chapters. DC electrical properties for temperature (100°C to 500°C) are measured and elaborated for the prepared samples. Results of Thermal analysis are also described in the end.

Chapter 8 is about discussion on summary of the results and conclusion. Research findings and major achievements, in comparison with literature have been

discussed in-length. Suggestions for suitability of prepared materials and their potential applications are also elaborated with reference to literature. In the last, future work has also been pointed out.

At last but not the least, Chapter 9 includes all the references used in this research dissertation.

Chapter 2

Synthesis Techniques of Magnetoplumbite Nanomaterials

Materials properties depend on their micro level structure, phase pure or impure nature, porosity level etc. Their properties are also influenced by the environmental conditions, types of dopants and the synthesis techniques. In the present work, we will synthesize magnetoplumbite samples series $SrFe_{12-2x}A_xB_xO_{19}$ and $SrFe_{12-x}B_xO_{19}$, by substituting divalent (A^{+2}), trivalent (B^{+3}) ions as dopants at octahedral Iron (B) site with a suitable proportion through wet-chemical methods. In general, two types of synthesis techniques are employed for the synthesis of M type Strontium hexaferrites. These are as followings

1) Top-Down approach
2) Bottom-up approach

2.1 Top-Down Approach

For synthesis of nano ferrites with this approach, the bulk material is breakdown to required level of nano scaled. The nano particles are synthesized by applying uniform high pressure through milling techniques [52] however it also has some defects associated with the surface of prepared materials like imperfections, contaminations etc. Top-down technique is further classified into following techniques

a) Ball milling method
b) Laser Ablation method
c) Arc discharge Method

2.2 Bottom-Up Approach

Bottom-up approach is based on the atomic scale combination of atoms which results into layer formation and these layer combine to form desired Nano level structures. This technique requires a self-assembly approach. Owing to the fewer defects, particle size control and crystalline shape etc., Bottom-up approach is preferred over top-own technique [53]. However, this approach finds it difficult to remove the solvents used in it which causes chemical or physical instability in results. This Problem is overcome by adding various types of stabilizers. The schematic flow diagram of top-down and bottom-up approaches are given in figure 2.1.

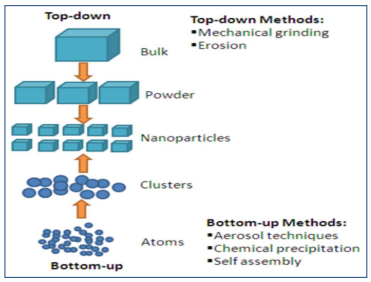

Fig 2.1: Schematic diagram of Top-down and Bottom-up Techniques [54]

2.2.1 Wet Chemical Techniques

Bottom-up technique can be routed through wet chemical methods. A few are mentioned below.

a) Composite Mediated Hydrothermal Method
b) Micro emulsion method
c) Sol-gel method
d) Co-precipitation Method

2.2.1.1 Composite Mediated Hydrothermal Method

This method is carried out in a Teflon chamber which contains reactants and hydroxides (NaOH-KOH), on keeping them in a pre-heated oven. The process takes place at 170°C while NaOH-KOH behaves as a catalyst to increase the reaction rate and as precipitating agent. This process is very simple, echo friendly and does not involve much cost however it is different from hydrothermal method due to choose of different catalyst [55].

2.2.1.2 Micro Emulsion Method

In this method, emulsion which is an output medium consists of water and oil soluble components of desired materials. In order to execute the process reaction, different surfactants are also introduced into the emulsion which not only initiate the process reaction at nano scale but also help in controlling the size of water drops.

Introduction of surfactants into emulsion results into formation of oil and water connection. Water to surfactant molar ratio is important to control water droplets, known as reverse micelle. Reaction between Reverse micelle and the added reactants results into formation of nanoparticles of desired. For synthesis of M-type hexaferrites, different types of surfactants namely Cetyltrimethy-Lammonium-Chloride and Sodium-Dodecyl-Sulfate have been used by different researchers but some drawbacks have also been reported as high annealing time and requirement of bulk and sample quantities of liquids which make this type of method much costly [23].

2.2.1.3 Sol-gel Method

It is a modified form of sol-gel method. In this process system undergoes transformation from liquid to gel phase resulting into final powder shaped product upon removal of added solvents. This processing is much simple and is much cost effective as-well however its drawback is that it is not environment friendly [55]. The schematic of Sol-gel method is shown in figure 2.2.

In the present research work, sample series of pure $SrFe_{12}O_{19}$, $SrFe_{12-x}Cr_xO_{19}$ (x = 0.0, 0.2, 0.4, 0.6, 0.8, 1.0) and $SrFe_{12-2x}Cr_xZn_xO_{19}$ (x = 0.0, 0.2, 0.4, 0.6, 0.8, 1.0) were synthesized by Sol-gel method adopting following synthesis scheme. For Cr doped Strontium hexaferrites series, highly pure precursors materials $Cr(NO_3)_3 9H_2O$, $Fe(NO_3)_3 9H_2O$ and $Sr(NO_3)_2$ were properly weighed and dissolved in molar ratio (14:1) with ethylene glycol. However, for Cr-Zn doped Strontium hexaferrite series Zn hexahydrate were used as precursor materials. All were added along with other precursor materials, stated above. Then after that mixture was stirred for 30 minutes for obtaining homogeneity mixture. The mixture was put in environment of 70°C for up to 5 hours. For gel formation, the temperature was increased by 120°C. At 195°C, gel turned to dried powder form. The obtained powder was undergone for calcination process at temperature about 910°C for 20 minutes. After that it was sintered at 920°C the pellets were formed and then used for structural investigations.

2.2.1.4 Co-precipitation Method

It is an important technique used for synthesis of nano particles. It is very cost effective and echo friendly, plus the control over the particle size with changing environmental conditions like temperature, pH value and time, give an added advantage

[56]. Nucleation growth and agglomeration take place side by side during this process. During the nucleation process, the small size particles like precipitates are formed while during their growth process, they tend to combined together to form a particle of larger sizes and become more stable thermodynamically. During the process, nucleation rate must be higher than growth rate. Stirring speed, time of solution and pH values also effect the agglomeration, number of nucleation sites and growth rate.

In the present research work, $SrFe_{12}O_{19}$ and $SrFe_{12-2x}Cr_xZn_xO_{19}$ (x = 0.0, 0.2, 0.4, 0.6, 0.8, 1.0) were synthesized by Co-precipitation method adopting following synthesis scheme, as shown in figure 2.3. $Sr(NO_3)_2$, $Fe(NO_3)_3 9H_2O$, transition metal Chromium Nitrate and Zn hexahydrate precursor were weighted in proportionate ratio. After that they were mixed to dissolve in de-ionized water followed by magnetic stirring continuously. It formulated a homogenous solution. Stirring mixing of solution was done in the beaker and temperature was increased up to 70°C. Two moles of NaOH solution was found suitable to achieve the desired pH level of 12 which was added in the already prepared homogeneous solution at 70°C, with magnetic stirring still continue so that pH level may be fixed.

The solution starts transforming into brown colored precipitates. Upon heating the solution further on 70°C for about 45 minutes [57]. Then it is removed from hot plate to attain room temperature. Then, the next step is to remove the impurity or by-products which is carried out by washing the dried precipitates with de-ionized water so that pH level 8 is achieved. Next step is to dry the washed-out precipitates in an oven by setting the oven temperature at 105°C and hard clusters formed are crushed to fine powder. The prepared powdered sample is further calcined to 910°C for maximum 20 minutes. In the next step powder is transformed to pellets with the help of hydraulic press. After that, the pellets samples are taken to sintering oven for controlled sintering process which is carried out at 920°C with a temperature gradient of 10°C/minutes.

2.2.1.5 Process Flow Charts Sol-gel and Co-Precipitation synthesis Methods

The process flowcharts of the methods are shown in figures 2.2 and 2.3 respectively.

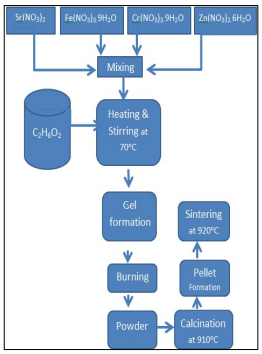

Fig 2.2: Flow chart of Sol-gel method

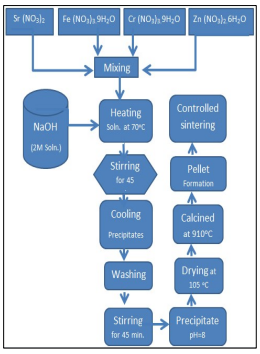

Fig 2.3: Flow chart of Co-precipitation method

Chapter 3

Characterization Techniques

In the present study, we will investigate the structure, electrical and thermal properties of M-type Hexaferrites and its different doped compositions $SrFe_{12}O_{19}$, $SrFe_{12-x}Cr_xO_{19}$, $SrFe_{12-2x}Cr_xZn_xO_{19}$ (x=0.0, 0.2, 0.4, 0.6, 0.8, 1.0). For structural and morphology characterization, X-ray Diffraction (XRD), X-rays Absorption Fine Spectroscopy (XANES and EXAFS), Fourier Transform Infrared Spectroscopy (FTIR) and Scanning Electron Microscopy (SEM) will be used. Electrical properties as a function of frequency and temperature will be studied and correlated with the structural information. Impedance analysis will be performed to understand the grain and grain boundary effect. Thermal properties of materials like volumetric heat capacity, thermal conductivity and the thermal diffusivity have been performed by using Advantageous Transient Plane Source (ATPS) method.

3.1 Structural Analysis

3.1.1 X-Ray Diffraction (XRD) Analysis

It is a useful non-destructive material characterization technique which is frequently used by scientists and engineers to investigate the materials at atomic level and to probe the crystallite size, surface morphology and phase analysis of crystalline, partially crystalline materials. However, non-crystalline materials can also be studied by this powerful technique. It is well established that XRD technique can be used for determination of crystallography of material like its structure, orientation, crystallite and grain sizes, lattice parameters, phase purity inter-planar spacing, stresses and strains in the lattices and crystal defects [58]. Its working principle is based on interaction of fast moving electron beam with the target material, leads to generation of X-rays, particular to that material. The geometrical illustration is given in figure 3.1 and schematic of a simple diffractometer is given in figure 3.2. Most of the XRD equipment use Cu as a target which strike on the surface of the sample material, placed for testing. Let us consider that for a sample material, d is the spacing between its lattice plane, and the wave length of the X-rays produced be λ, then by Bragg's law we can write that

$$\lambda = 2d\sin\theta \qquad (3.1)$$

Where θ is angle between the incident x-rays and crystal.

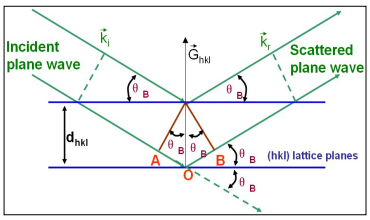

Fig 3.1: Geometrical illustration of Bragg's law [58]

For constructive interference, the path difference becomes integral multiple of wave length and above equation takes the form of

$$n\lambda = 2d_{hkl}\sin\theta \qquad (3.2)$$

where 'hkl 'are referred as Miller indices.

Crystallite size 'D' can be determined using Full Width at Half Maximum (FWHM), attained from the diffraction peaks in Scherrer's formula and is given as

$$D = \frac{k\lambda}{\beta\cos\theta} \qquad (3.3)$$

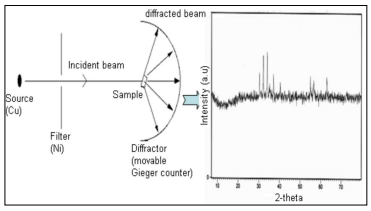

Fig 3.2: Schematic of simple X-ray Diffractometer [58]

Where λ, β and θ are the wave length, FWHM and Bragg's angle respectively.

Lattice constant can be determined formula and is given as

$$\frac{1}{d^2} = \frac{4}{3}\left[\frac{(h^2+hk+k^2)}{a^2} + \frac{l^2}{c^2}\right] \qquad (3.4)$$

Here d denotes, the inter planar-distance, hkl miller indices and lattice constants 'a' and 'c'. The volume V of the unit cell with lattice parameters 'a' and 'c' can be given as

$$V = \frac{\sqrt{3}}{2}a^2c \qquad (3.5)$$

The phase purity can be calculated by formula, as given below,

$$\text{Purity}\ (\%) = \left(\frac{I-I_0}{I}\right) \times 100 \qquad (3.6)$$

Where, I and I_0 are the sums of intensities and same phase intensities respectively.

The theoretical density or X-ray density can be described as

$$\rho_{th} = \frac{nM_m}{VN_A} \qquad (3.7)$$

Here parameters in above equation are, 'n' number of formula units in a unit cell, 'M_m' molar mass, 'V' volume of unit cell and 'N_A' is the Avogadro's number which is equal to 6.02×10^{23}. Experimental density can be determined by,

$$\rho_{exp} = \frac{m}{V} \qquad (3.8)$$

Where, m is the mass and V is the volume of the cell.

Porosity in the material can be calculated as

$$P = \left(1 - \frac{\rho_{exp}}{\rho_{th}}\right) \times 100 \qquad (3.9)$$

Where, ρ_{th} and ρ_{exp} represent theoretical and experimental densities respectively.

Stress and Strain can be calculated by famous Williamson-Hall analysis technique. We used Uniform Deformation Model (UDM) for the estimation of lattice strains for the prepared powdered samples. UDM suggests that the crystal is of isotropic in nature. Following relation can be used to calculate the lattice strain emerged because of crystal imperfection

$$\epsilon = \frac{\beta_{hkl}}{4\tan\theta} \qquad (3.10)$$

Equation (3.3) and (3.10) give,

$$\beta_{hkl} = \frac{k\lambda}{D\cos\theta} + 4\epsilon\tan\theta \qquad (3.11)$$

On re-arranging above equation (3.11), we get

$$\beta_{hkl}\cos\theta = \frac{k\lambda}{D} + 4\epsilon\sin\theta \qquad (3.12)$$

Equation (3.12) represents famous Williamson-Hall (W-H) equation [59]. All of the plots for samples have been generated with the help equation (3.12). The slope of the line tells about the lattice strains and their average values.

3.1.2 Fourier Transform Infrared Spectroscopy (FTIR)

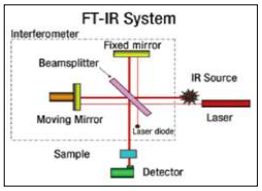

Fig 3.3: Working Principle of FTIR [60]

Fig 3.4: An example of an FTIR Spectrometer [61]

It is technique, used for getting an infrared spectrum of absorption or emission of material in either form a solid, liquid or gas [60]. With the help of an FTIR, we can simultaneously get a high-spectral-resolution data for a wide spectrum. The infrared spectroscopy data obtained is in raw form which is collected as result of constructive interference and processed for Fourier Transformation for actual spectrum. FTIR tells about chemical compositions and nature of bonding of samples either in solid, liquid or gas form.

FTIR identifies the types of chemical bonding in a molecule by generating a spectrum infrared absorption nature which is like a molecular "fingerprint". The wavelength of absorbed light is associated with the type of chemical bond, referred to the annotated spectrum.

Working principle of FTIR is explained and shown in figure 3.3. It involves study of electromagnetic fields (EM) interactions with matter in IR spectra region. EM waves couple with the molecular vibrations and excite them to a higher state. The IR frequency absorption takes place at a certain frequency upon its interaction with the molecules. FTIR spectroscopy is sensitive for chemical composition of the sample material and uses fingerprint technique. Example of modern FTIR equipment is shown in figure 3.4.

3.1.3 X-ray Absorption Fine Spectroscopy (XAFS)-Analysis

X-Ray Absorption Fine Spectroscopy (XAFS) is a powerful and unique technique to probe local structure of a specific element. This is a modern technique to investigate the atomic structural features of an element. One can get information about the valence

The Art of writing only for samples use

state, bond lengths, coordination numbers and nature of neighboring atoms. There are many review articles available on this technique, which are very useful to understand the theory, tools and applications of XAFS. XAFS working principle and process as shown in fig 3.7-3.8, are based on the attenuation of a monochromatic beam of x-rays of energy E, which on passing through a homogenous sample having thickness t can be expressed by Beer-Lambert's law [62]

$$I(E) = I_o E e^{-u(E)t} \quad (3.13)$$

Here $I_o(E)$ and I(E) are regarded as X-ray intensities for incident and transmitted mode respectively. Linear absorption coefficient μ(E) gives probability X-rays absorption.

Fig 3.5: ELLETRA Synchrotron Lab and storage ring

Fig 3.6: ELLETRA XAFS Beam Line

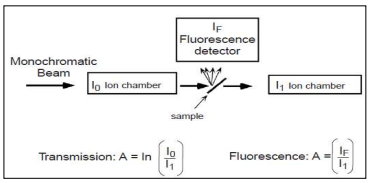

Fig 3.7: Schematic of XAFS [62]

When the energies of absorbed radiations become equal to binding energies of electrons in K, L_1, L_2 etc shells, it results in generation of absorption edges of elements. The oscillatory features are produced above the edges called XAFS and gives penalty of information regarding local structure. The fine spectra be classified in two energy regions one which occurs about 50 eV above edge is called XANES (X-ray absorption

The Art of writing only for samples use

Near Edge Fine Structure) while the second region from 50eV to 1000 eV post edge is called EXAFS (Extended X-ray Absorption Fine Structure).

3.1.3.1 X-ray Absorption Near Edge Fine Spectroscopy (XANES)

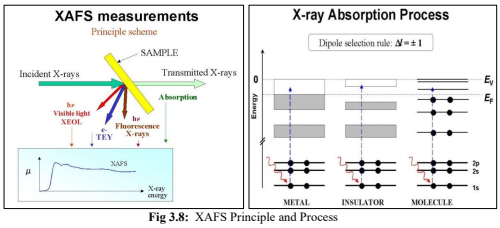

Fig 3.8: XAFS Principle and Process

XANES signal has a much larger signal than EXASF. A XANES spectrum is originated due to multiple scattering from the first shell of absorbing atom and also from the multiple scattering of distant atomic shells. XANES interpretation is complicated due to a number of reasons. First of all XANES lack physical or analytical description secondly the EXAFS equation does not hold good or remain valid for low k values. At low k , mean free path is increased. XANES provides information regarding site symmetry and oxidation state of absorbing atoms.

3.1.3.1.1 XANES Features and Information

XAFS is an element specific technique used to study many structural features from the edge, pre-edge region and oscillation about 50 eV above edge. XANES spectra being close to the absorption edge involve majorly multiple scattering. XANES being a finger printing technique, also tells about the oxidation or valence state of absorbing atom. For that purpose, shift in the absorption edge energy or simply the chemical shift is helpful by comparing the same edge shift data with already available beam line data for the same edge shift and different oxidation state of metal can be can estimated.

3.1.3.1.1 Chemical shift and Oxidation State

Change in the absorption edge of a metal in a compound from change of edge position in pure element state is known as chemical shift.

The Art of writing only for samples use

$$\Delta E_i = E_i(\text{compound}) - E_i(\text{element}) \quad (3.14)$$

The shift ΔE is positive edge shift towards higher energy region range can vary from 1eV to 15eV. Upon formation of a compound , the valence electron are redistributed among atom (cations and anions) with flow of charge from metal ions (cations) to other ligand atom (anion) which results in an increase in the binding energy of inner shell electron on increasing effective nuclear charge. It results in shifting of corresponding absorption edge to the higher energy side as compared to the edge energy in pure metal. This indicates an increase oxidation state. Change of edge can be determined by several methods but usually point first maximum peak of derivative absorption curve is considered a reliable edge energy position.

3.1.3.2 Extended X-ray Absorption Fine Spectroscopy (EXAFS) Analysis

EXAFS ranges about 50eV to 1000 eV post edge region due to single scattering events from the (5Å-6Å) from absorbing atom and provides information regarding chemical environment of neighboring atoms, site occupancy, interatomic distance of surrounding atoms and distortion in the crystal structure. The EXAFS equation can be expressed as [62]

$$\chi(k) = S_o^2 \sum_i [N_i F_i(k)/kR_i^2] \, \mathrm{Sin}[2kR_i + \emptyset_i(k)] \exp(-2\sigma_i^2 k^2) \exp[-2R_i/\lambda(k)] \quad (3.15)$$

Here, the quantity χ(k), can be defined as the oscillations in terms of photo-electron wave number, and is simply referred "the EXAFS". The parameters in above equation (3.15) can be termed as N is Coordination number of atoms, $F_i(k)$ is effective scattering amplitude, φ(k) is phase shift, and λ(k) is mean free path of the photoelectron, respectively as functions of wave-vector k. The term R_i is the half path length of the photoelectron (i.e., the distance between the absorber and a coordinating atom for a single- scattering event.σ^2 defines the mean-square disorder of atom distance. If we know the properties of $F_i(k)$, φ(k) and λ(k) parameter, We can measure bond distance R, coordination number N and atomic disorder σ^2 for any element. A typical XAFS spectrum has been shown in figure 3.9.

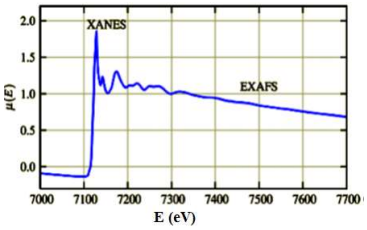

Fig 3.9: A Typical XAFS Spectrum [62]

3.1.4 Scanning Electron Microscope (SEM)

SEM uses a focused beam of electrons over sample surface for generation of a high-resolution image, whereas a simple microscope uses light for the purpose. The image created by the SEM can give information about the material's chemical composition and surface topography. SEM consists of following main components

- Electrons Source
- A downward column down through which electrons travel under the effect of electromagnetic field and lenses
- Electron detector
- Sample chamber
- Computer and screen for images display

Electrons source creates and injects the electrons downward in the column through the combination of different magnetic lenses forming a focused electrons beam. Beam strikes at the sample surface, placed inside chamber. The column and chamber are operated through pumps to maintain the desired vacuum level. Vacuum level is related with design of microscope. A Schematic of a Scanning Electron Microscope is shown in figure 3.10. Scan coils function is used to control position of electron beam and also helps the beam to scan over the sample surface. It collects the desired information of sample target area. Secondary electrons emission takes during interaction of electron beam with sample surface, in the form of signals which are detected by different suitable detectors and image is formed. These images can be seen on display screens.

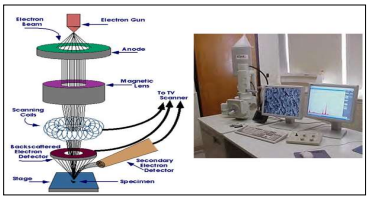

Fig 3.10: Schematic of a Scanning Electron Microscope

3.2 Electrical Properties

Electrical properties are measured in terms of AC electrical response and DC electrical response and accordingly analysis are performed. AC electrical properties such as dielectric constant, dielectric loss, conductivity, impedance etc. with the varying effect of the operating frequency whereas for DC electrical response, electrical resistivity of material is measured at a fixed frequency, under changing the temperature conditions.

3.2.1 AC Electrical Properties

In order to measure the electrical response with respect to changing frequency, a precision component analyzer (6400B) can be used. The response can be measured in two ways either by two probe method or by using four probe methods. The selection of method depends on the lower or higher value of resistivity of the material as explained above. The equipment frequency ranged from 20Hz - 3MHz. Voltage level can be set from 1mV to 10Vrms to derive the instrument. The parameters like AC conductivity, dielectric loss, dielectric constant, impedance its imaginary and real part can be measured by keeping the temperature fixed at a certain value, with respect to changing frequency. The electrical responses can be measured from Room temperature value to 500ºC. Dielectric constant can be given as,

$$\epsilon' = \frac{Cd}{\varepsilon_0 A} \tag{3.16}$$

Where A is the area of material in the sintered pellet form, ε_0 is permittivity equal to 8.854 F/m. Also, the parameter d is the material thickness and C defines capacitance which is measured using Precision component analyzer.

Dielectric constant value of a material also explains about the charge storage capacity of that material. This property is associated with the polarization mechanism

which takes place upon applying electric field due to exchange of Fe^{2+} and Fe^{3+} ions. Applied electric field causes the charge carriers to accumulate across grain boundaries of the material which give rise to space charge polarization. When the charge carriers start aligning themselves with the applied field, a slight shift from the equilibrium position occurs to them. Such type of polarization is referred to as Dipolar polarization. These positive and negative produced ions tend to move in the opposite directions. This effect generates ionic polarization. The polarization caused by positive (nucleus) and negative (electrons) displacement, in a direction opposite to each other is known as electronic polarization. The emergence of different polarization mechanism takes place at high frequencies, because charge carriers are not capable enough to withstand applied electric field. Different polarizations governing at lower frequencies have been shown in figure 3.11.

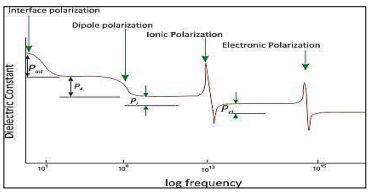

Fig 3.11: Different types of polarization present at lower frequencies

Polarization can be measured by the following simple formula,

$$P = N \propto E \tag{3.17}$$

Where, parameter P is polarization, N represents the no. of charge carriers ions, atom or molecules, α represent Polarizability and E is referred to as applied field.

Another important property associated to dielectric materials is the tangent loss or the Dielectric loss. It gives information about energy dissipation response upon application of external electric field with the material. These energy losses are comparatively higher in the material at lower frequencies due to re-orientation and relaxation of charge carriers but low at higher frequency due to their unresponsive characteristics to the applied field. Dissipation factor or tangent loss can be measured with the help of LCR meter and is given by the formula,

$$\tan\delta = \frac{\epsilon''}{\epsilon'} \tag{3.18}$$

Where, the term ε'' represents dissipated energy, ε' represent the amount of the energy deposited in the sample material per cycle.

AC conductivity can be given as,

$$\sigma_{AC} = \omega\varepsilon_0\varepsilon' \tan(\delta) \tag{3.19}$$

Where, the term ω defines angular frequency in the relation. It can be expressed as $\omega = 2\pi f$. The term ε_0 is the free space permittivity. The term ε' is dielectric constant and tan (δ) represent dissipation factor. In General, conductivity is expressed by relation

$$\sigma_{tot} = \sigma_o(T) + \sigma(\omega, T) \tag{3.20}$$

Here σ_o (T) and σ(ω,T) are the DC conductivity due to band conduction and AC conductivity due to hopping process respectively. The AC conductivity can be expressed as

$$\sigma_{AC}(\omega, T) = B\omega^n \tag{3.21}$$

It is famous Jonscherr's Power Law. In this expression ω is frequency. B and n are constant quantities associated to temperature and compositions. By using value of n, it can be helpful to define and relate different theoretical model regarding conduction mechanism in the material. Impedance parameter which gives a measurement of the total impedance to the electrons motion for the flow of current at any frequency has two parts. One real, referred to as Resistance R and other Reactance, referred to as X. The relation between real and imaginary parameters of Impedance, in terms of rectangular coordinates can be given as Z = R+ jX. Admittance (Y) is given by the simple relation of Y = 1/Z. The expression for admittance terms can be expressed as Y= G + jB. Here, G and B can be reoffered as Conductance and Susceptance of the material.

Resistance offered by the grain and grain boundaries in the material is studied by analyzing the impedance response of the materials. Impedance response is studied as in-whole as the study of the different parts Capacitive and reactance and resistance of ac circuit together. As explained earlier, the Real part which corresponds to the resistance, is given by the relation

$$Z' = Z\text{Cos}\theta \tag{3.22}$$

The impedance Imaginary part is referred as reactance and can be calculated by the following formula, given by

$$Z^* = Z\text{Sin}\theta \tag{3.23}$$

3.2.2 DC Electrical Response

We preferred two probe methods for measuring DC electrical response of all the synthesized sample material. We measured DC resistivity and conductivity properties of the material. The measurement of resistance was performed using Wayne Kerr LCR meter 6440B, from 100ºC Temperature to 500ºC. Resistivity of the material can be calculated by using the relationship,

$$\rho_{DC} = {}^{RA}/_{L} \quad (3.24)$$

Here, R, A and T stands for the measured quantity of resistance, area and sample thickness. In order to calculate activation energy (E_a) of the samples, Arrhenius relation can be helpful. Arrhenius relation can be given as

$$\rho = \rho_o \exp\left(\frac{E_a}{k_B T}\right) \quad (3.25)$$

In the above relation, E_a is regarded as activation energy, ρ is DC resistivity at T temperature, k_B is considered as Boltzmann's constant and the parameter ρ_o gives resistivity at 1/T=0. Also, DC Conductivity can be given as

$$\sigma_{DC} = {}^{1}/_{\rho_{DC}} \quad (3.26)$$

3.2.3 Two Probe Method

For materials of higher resistive nature two probe method is used. Schematic of two probe method is shown in figure 3.12. Powdered sample material pressed into pellet form with the help of hydraulic press, and then it is placed properly between two copper plates. The Copper plates are connected with LCR meter, in series combination with an AC or DC source.

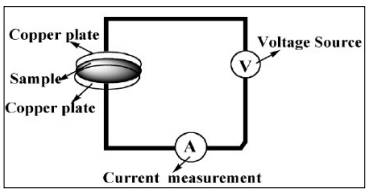

Fig 3.12: Schematic of Two Probe method

The Art of writing only for samples use

3.3 Thermal Transport Properties

Transient-Plane Source (TPS) Technique is helpful in measuring thermal transport properties with varying temperature. The modern technique used for this purpose is, Advantageous Transient Plane Source (ATPS) in which test sample in thermal equilibrium with atmosphere is provided heat pulses with different times and temperature gradient is measured. Heat flowing into the sample from three different dimensions can be examined via a heat source and temperature sensor, based on TPS technique. With each degree change (increase or decrease) in temperature, the electrical resistance also gets change. The quantities, increase in temperature ΔT and electrical resistance are time-dependent parameters which can be described as following [63]

$$R(t) = R_o\,(1 + \alpha\Delta T(\tau)) \quad (3.27)$$

Where α is the temperature coefficient of resistivity (TCR), R_o is TPS element resistance and $\Delta T(\tau)$ is the mean value of increase in temperature of TPS element. Parameter (τ) is a dimensionless variable. (τ) can be given by;

$$\tau = \sqrt{\frac{t}{\theta}} \quad (3.28)$$

and

$$\theta = \frac{r^2}{k} \quad (3.29)$$

here't' is transient heating starting time. k is given as thermal diffusivity parameter and θ is characteristic time and r is a constant which gives information about overall resistive pattern. Similarly, thermal diffusivity (k), thermal conductivity (λ) and volumetric heat capacity (ρCp) can be given as by following relation.

$$k = \frac{\lambda}{\rho C_p} \quad (3.30)$$

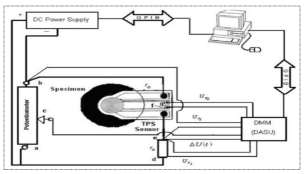

Fig 3.13: Schematic diagram of ATPS [63]

The Art of writing only for samples use

Chapter 4

Study of Structural and Conduction Properties of $SrFe_{12}O_{19}$

The Art of writing only for samples use

Co-precipitation method is one of the most classical and convenient type of chemical route to prepare nanoparticles. It is cost-effective and eco-friendly synthesis technique. It does not require a high temperature so is suitable for industrial purposes. Another method, Sol-gel, is also type of chemical route method used to synthesis nanoparticles. It is based on the formation of solution and gel. Crystallinity of the material can be improved by heat treatment method. It is less time taking as compared to co-precipitation method. Also, it gives good control on the particle size. No surfactants are used in it so it offers better homogeneity.

During our research, magnetoplumbite ($SrFe_{12}O_{19}$) hexaferrites samples were prepared by Sol-gel and Co-precipitation methods, to study their effects on material structural and transport properties. X-Ray Diffraction (XRD), Fourier Transform Infrared Spectroscopy (FTIR), and Scanning Electron Microscopy (SEM) were used to understand the structure and morphology of the prepared samples. Electrical properties with respect to frequency and temperature were studied. All the measurements were taken at frequency range from 1 kHz to 3-MHz and the temperature range from 100ºC to 300ºC. At fixed frequencies of 500 kHz and 1-MHz, material's dielectric behavior was also investigated. Impedance analysis for the prepared samples was also carried out. Real and Imaginary parts of impedance were studied. Cole-Cole plots were drawn to understand the grain and grain boundary effects in the pure $SrFe_{12}O_{19}$ samples. DC resistivity of the materials was also measured in the temperature range from 100ºC to 500ºC.

4.1 Structural Analysis

4.1.1 X-Ray Diffraction (XRD) Analysis

Structural analysis of magnetoplumbite samples of $SrFe_{12}O_{19}$, prepared by Sol-gel and Co-precipitation methods was done by using X-Ray Diffraction Spectroscopy Radiation source Cu –Kα having the wavelength 1.54Å. The selected 2θ range was from 20º to 80º. In figure 4.1, indexed XRD pattern of sintered samples of magnetoplumbite Sr-hexaferrite are shown. The sample prepared by Sol-gel method was sintered at 920ºC and sample prepared by Co-precipitation method was sintered at 920ºC for ten minutes with temperature gradient of 10ºC/minute. The observed peaks were matched with the reference card no 00-033-1340. The lattice parameters 'a' and 'c', crystallite size (D) and volume of a unit cell (V) were calculated by using equations

(3.4) , (3.3) and equation (3.5) as explained earlier. The expansion in the unit cell volume may be due to the effect of stresses and strain. Hexagonal structure was observed. Peaks of αFe_2O_3 were also seen in sample material prepared by both methods. All the values calculated by XRD are shown in table 4.1.

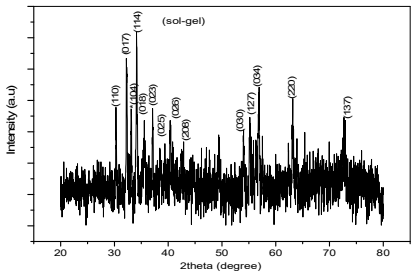

Fig 4.1(a): XRD Pattern of magnetoplumbite Strontium hexaferrite prepared by Sol-gel method

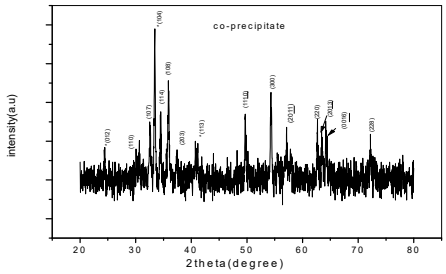

Fig 4.1(b): XRD Pattern of magnetoplumbite Strontium hexaferrite prepared by Co-precipitation method

Table 4.1: Lattice parameters of $SrFe_{12}O_{19}$ prepared by Sol-gel and Co-precipitation method

	$SrFe_{12}O_{19}$ (Sol-gel method)	**$SrFe_{12}O_{19}$ (Co-precipitation method)**
a (Å)	5.88(9)	6.0(1)
b(Å)	5.88(9)	6.0(1)
c(Å)	23.071(3)	22.99(8)
Volume $(Å)^3$	692.58(1)	720.5(9)
$D_{(max\ int)\ (nm)}$	67	67

4.1.2 Fourier Transform Infrared Spectroscopy (FTIR) Analysis

Figure 4.2 (a) and figure 4.2 (b) represent the FTIR spectra of Sr-hexaferrites prepared by two synthesis techniques at the frequency range from 500cm^{-1} to 4500cm^{-1} .The bands range between 400 cm^{-1} -1500 cm^{-1} represents the existence of Strontium hexaferrites [64].

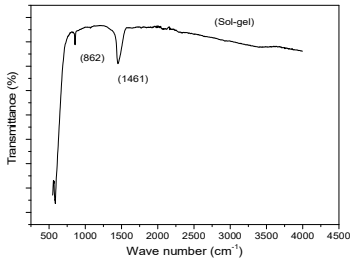

Fig 4.2 (a): FTIR spectra of $SrFe_{12}O_{19}$ prepared by Sol-gel method

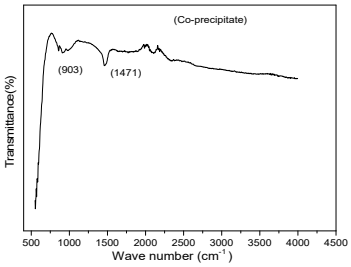

Fig 4.2 (b): FTIR analysis of $SrFe_{12}O_{19}$ prepared by Co-precipitation method

4.1.3 Scanning Electron Microscope (SEM) Analysis

Figure 4.3(a) and 4.3(b) shows SEM micrographs of $SrFe_{12}O_{19}$ prepared by two identified methods. Due to high surface area to volume ratios, particles agglomerated themselves to lessen or minimize their surface energy.

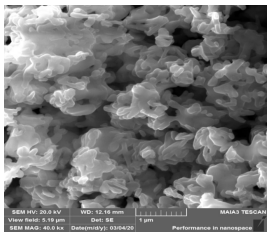

Fig 4.3(a): $SrFe_{12}O_{19}$ prepared by Sol-gel method

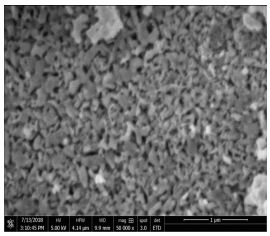

Fig 4.1.3 (b): $SrFe_{12}O_{19}$ prepared by Co-precipitation method

4.2 AC Electrical Properties with respect to Frequency and Temperature

4.2.1 Dielectric Constant (ϵ′)

Figure 4.4 represents the samples prepared by Sol-gel and Co-precipitation methods. Variation in dielectric constant with respect to frequency and temperature was investigated. The selected temperature range was from 100°C to 300°C. The frequency range was from 1-kHz to 3-MHz. The dielectric constant was observed to be increased with increase in temperature. At lower frequencies, high value of dielectric constant was observed. The reason behind this effect could be polarization phenomena [65]. All types of polarizations take an active part during this effect. Also, electron hopping is maximum at low frequency. At high frequencies, electrons could not show successful hops as a result of which polarization dies out.

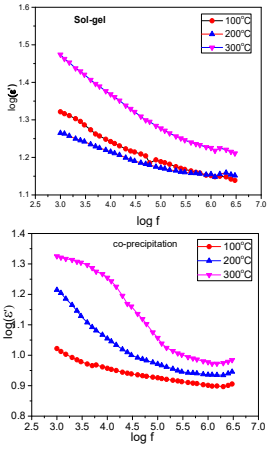

Fig 4.4: Variation in dielectric constant with respect to frequency and temperature for $SrFe_{12}O_{19}$

The high value of dielectric constant observed at 100°C for sample prepared by sol-gel method might be due to the greater number of ferrous ions at interstitial site. At a temperature of 300°C and a frequency of 1 kHz, sample prepared by Sol-gel method

showed dielectric constant value 29.51 whereas the sample prepared by co-precipitation method had dielectric constant value 21.13.

4.2.2 Dielectric Loss Tangent (tanδ)

Loss tangent is the dissipated part of the energy. This is the energy which may not come back and becomes part of the system. Figure 4.5 shows loss tangent plots for samples prepared by two different methods. The maximum value of losses observed was at lower frequencies. The increased in the frequency range effect the loss tangent and loss get start decreasing. At high temperatures, higher losses were observed for the samples. Relaxation peaks were also observed at temperature of 100°C for both the samples. It might be since at this temperature, applied and oscillation frequencies of the materials get simply match and as result relaxation peaks are observed. At a temperature of 300°C and frequency of 1 kHz, loss tangent of sample material prepared by sol-gel method is 0.30 whereas sample prepared by Co-precipitation method showed higher value of loss that is 5.28.

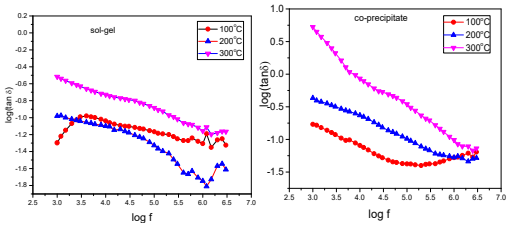

Fig 4.5: loss tangent plot for Strontium hexaferrite

4.2.3 AC conductivity (σ_{AC})

Figure 4.6 represents AC conductivity plots for the $Srfe_{12}O_{19}$ samples synthesized by Sol-gel and Co-precipitation methods. The graphs obeyed the universal Jonscher's Power law [66]. Dispersion region was observed for all the selected temperature range. By increasing the frequency and temperature, conductivity of the materials boosts up. Thermal energy enhanced the process of polarization in magnetoplumbite ferrites

prepared by Sol-gel and co-precipitation methods. Electron exchange interaction between the Fe^{+2} and Fe^{+3} increased. All of it resulted in the increased of conductivity of the material.

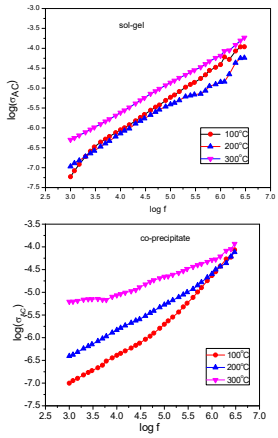

Fig 4.6: Represents the AC conductivity of $SrFe_{12}O_{19}$ prepared by Sol-gel and co-precipitation methods

4.2.4 Impedance (Z)

In order to understand the effect of grain and grain boundary, the impedance spectroscopy was used. The selected temperature range was from 100°C to 300°C. The frequency used was from 1 kHz to 3-MHz.

4.2.4.1 Real Part (Z′) of Impedance

In figure 4.7, real parts of the complex impedance for both samples are plotted. The value seems to be decreased by increasing the value of temperature for both the samples. The grain boundaries effect was observed less active at higher temperature. More and more electron hops between the sites resulting in decrease of impedance.

However, at lower frequencies, due to the effectiveness of all polarizations, high value of impedance was observed.

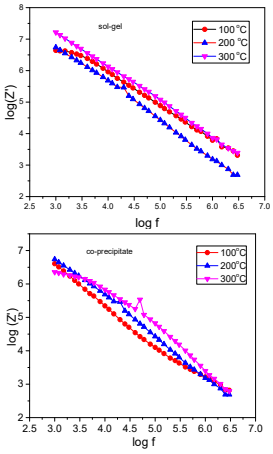

Fig 4.7: Real part of the complex Impedance for $SrFe_{12}O_{19}$ prepared by Sol-gel and co-precipitation methods

4.2.4.2 Imaginary Part (Z′′) of Impedance

Figure 4.8 shows the imaginary part of the complex impedance of strontium hexaferrite samples at different temperatures prepared by Sol-gel and Co-precipitation methods. This part of impedance showed the same trend as that of real part. Decrease was observed with respect to increase in frequency for both the samples prepared by different routes relaxation peaks were observed.

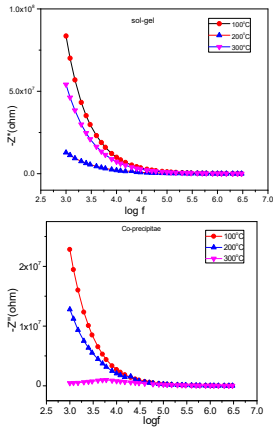

Fig 4.8: Imaginary part of the complex impedance for Strontium hexaferrites prepared by Sol-gel and co-precipitation methods

4.2.5 Cole-Cole Plots

Figure 4.9 shows Cole-Cole plot for the samples of $SrFe_{12}O_{19}$ prepared by Sol-gel method and Co-precipitation methods. The frequency range selected is from 1 kHz to 3-MHz. the plots are drawn at different Temperatures (100°C to 300°C) to understand the conduction mechanism in magnetoplumbite structure. By increasing the temperature, the diameter of the arcs seems to be reduced. This might be due to the relaxation process [67]. These incomplete semicircle arcs represent the bulk effect in the system.

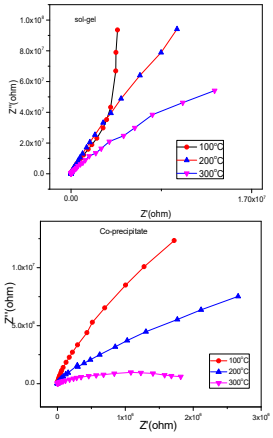

Fig 4.9: Cole-Cole plots for $SrFe_{12}O_{19}$ samples prepared by sol-gel and co-precipitation method

4.3 Electrical Analysis at Fixed Frequencies of 500 kHz and 1-MHz

4.3.1 Dielectric Constant (ϵ′)

At a fixed frequency of 500 kHz and 1-MHz, dielectric properties were measured. The temperature range was from 100°C to 500°C. In figure 4.10, it is clearly shown that the value of dielectric constant for both the frequencies increased by increasing the temperature. However the higher value of dielectric constant is observed at 500 kHz. Since the frequency is kept constant so in present case, main role is played by temperature. At a certain value of temperature, the phase transformation was observed for $SrFe_{12}O_{19}$ prepare by both methods. This critical temperature was observed to be exist between 400°C to 500°C. This is called the transition temperature. At this temperature, the material converted from ferroelectric to paraelectric. Such a behavior is already reported in hexaferrites [67,69].

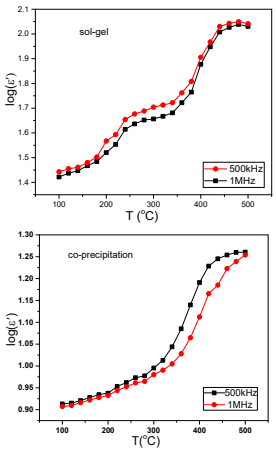

Fig 4.10: Dielectric Constant at 500 kHz and 1-MHz frequencies for $SrFe_{12}O_{19}$ samples

4.3.2 Dielectric Loss Tangent (tan δ)

In figure 4.11, loss or Tangent delta plots are shown at a fixed frequency of 500 kHz and 1 MHz .The value of tangent losses increased by increasing the temperature for both the frequencies. Increased hopping rate due to the temperature, boosted up the process of polarization. The dielectric constant and the tangent loss nearly follow the same trend. Relaxation peaks were observed for the samples prepared by sol-gel method.

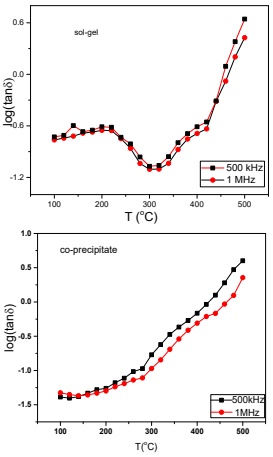

Fig 4.11: Loss tangent (tanδ) at 500 kHz and 1 MHz frequencies for $SrFe_{12}O_{19}$ samples

4.3.3 AC Conductivity (σ_{AC})

In figure 4.12, AC conductivity of the prepared Strontium hexaferrites samples is shown. The relaxation peak was observed at both the fixed frequencies for the sample prepared by Sol-gel method. The plateau part was observed at 500 kHz and 1-MHz frequencies for the samples prepared by co-precipitation method. This is independent of frequency effect. After that the dispersive part of the material was observed in between the temperature range of 100°C to 500°C. The heat energy increased the process of conduction. The successful hopping of electrons between octahedral (B) to octahedral (B) sites, enhanced the conduction mechanism.

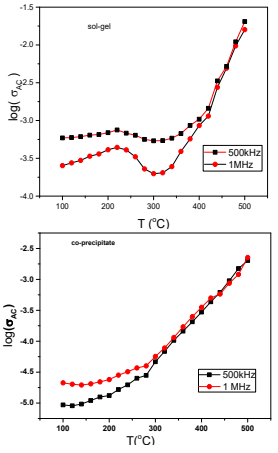

Fig 4.12: AC conductivity at 500 kHz and 1-MHz frequencies for $SrFe_{12}O_{19}$ samples prepared by Sol-gel and co-precipitation methods

4.3.4 Impedance (Z)

Figure 4.13 shows impedance plots at two fixed frequencies of 500 kHz and 1-MHz for $SrFe_{12}O_{19}$ samples prepared by Sol-gel and co-precipitation methods. The magnitude of impedance was observed to be decreased by increasing the temperature and frequency. Higher value of impedance was investigated as compared to that of 1-MHz. At 500 kHz and temperature of 100°C the value of Sol-gel prepared Strontium magnetoplumbite is found to be 1.265 $x10^5$ Ohm whereas the co-precipitation sample showed less value of impedance 6.032$x10^4$ Ohm.

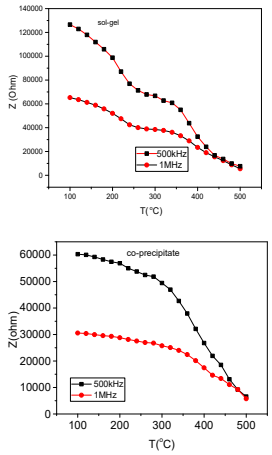

Fig 4.13: Impedance plots at 500 kHz and 1 MHz for $SrFe_{12}O_{19}$ samples prepared by Sol-gel and Co-precipitation methods

4.4 DC Resistivity

In figure 4.14, DC resistivity plots are shown for Strontium hexaferrite. It is clear from the figure that two activation regions were observed for both the compositions. This might be due to the distortion in hexaferrites lattice [67]. Presence of stresses and strain could also be the reason behind this. The activation energies of the prepared samples were calculated by using the Arrhenius relation. The slope of the equation gives the value of activation energy. The value lies between 0.12eV to 1.22eV for sample, prepared by Sol-gel method, whereas for the sample prepared by co-precipitation method, it was found to be lie in the range of 0.13eV to 1.00 eV.

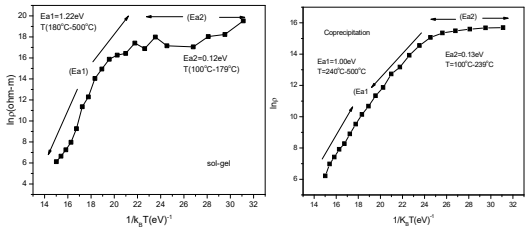

Fig 4.14: Arrhenius plots of Strontium hexaferrites prepared by Sol-gel and Co-precipitation methods

4.5 Conclusion

Samples were prepared by two methods sol-gel and co-precipitation. Both synthesis methods showed the hexagonal structure with presence of αFe_2O_3 however the intensity of hematite is higher in samples prepared by co-precipitation method. The maximum intensity crystallite size was found to be 67nm for both the samples. FTIR Analysis showed the formation of magnetoplumbite structure. SEM images showed the agglomeration of particles for both the samples. The highest value of dielectric constant 29.51 was observed for sample $SrFe_{12}O_{19}$ prepared by sol-gel route. The samples prepared by co-precipitation method showed dielectric value 21.13 at a temperature of 300°C and frequency of 1 kHz. The losses in sample prepared by Sol-gel method were 0.30 only whereas for co-precipitation route, it was observed to be 5.28 only. Impedance of the sol-gel sample at 500 kHz was 126543 Ohm whereas for co-precipitation it was 60328 Ohm. Two activation regions were observed for both the compositions due to the distortion in hexaferrite lattice.

Chapter 5

Study of Structural and Conduction Properties of $SrFe_{12-2x}Cr_xZn_xO_{19}$ (x = 0.0 to 1.0) prepared by Co-precipitation Method

In magnetoplumbite structure, by means of charge carrier concentration, we can control the losses. When Zn^{+2} is doped in M-type hexaferrites it tries to replace Fe^{+3} ions present at Tetrahedral (A) site. Due to charge neutrality condition, Fe^{+2} present at Octahedral (B) site are converted into Fe^{+3} which decreases the Fe^{+2} ions concentration in the whole structure. It leads the reduction in dielectric loss. It is also reported in literature that Cr^{3+} increased the functioning of high frequency devices. By keeping these things in view Cr^{3+} and Zn^{2+} combination was used to make the material suitable for high frequency appliances. Among magnetoplumbite $MFe_{12}O_{19}$ (M= Pb, Ba, Sr, Ca) hexagonal ferrites, Strontium hexaferrites are famous due to their excellent properties like high electrical resistivity, less eddy current losses [70], chemical stability [71], better thermal durability and outstanding magnetic properties [72,73].The beauty of magnetoplumbite Strontium hexaferrites structure is that its structural , electrical and dielectric properties can be tailored with a number of techniques like introducing different dopants and their concentration, environment, sintering temperature, cationic-distribution, particle sizes and synthesis methods [74]. In the present study the effect of synthesis technique on the structural and electrical properties of magnetoplumbite structure was tried to reveal. The famous co-precipitation method was used.

5.1 Structural Analysis

5.1.1 X-ray Diffraction (XRD) Analysis

Magnetoplumbite structures of $SrFe_{12-2x}Cr_xZn_xO_{19}$ (x=0.0, 0.2, 0.4, 0.6, 0.8, 1.0) were obtained by sintering the samples at 920°C for ten minutes with temperature gradient of 10°C/minute. Figure 5.1 showed the indexed pattern of XRD graph of Cr-Zn doped M type Strontium hexaferrites. Miller indices (hkl) and Crystallite size was determined by Scherrer formula as given in equation (3.3). Calculated crystallite size ranged from 42-67 nm. The different other structural parameters are also given in table 5.1. Lattice parameters revealed nonlinear response independent of Cr-Zn doping for $SrFe_{12-2x}Cr_xZn_xO_{19}$ series. Lattice parameters were observed to be reduced up to composition x = 0.6 due to distortion in crystal lattice [75]. Unit cell volume is also found to be decreased accordingly. After sample composition x = 0.6, lattice constant starts increasing. Fe^{+3} has ionic radii 0.67Å, higher than that of Cr^{+3} which is equals 0.63Å. Due to exchange of Fe^{+3} and Cr^{+3} charges, overall Magnetoplumbite crystal structure of Strontium hexaferrites contracts [76]. In Magnetoplumbite structures,

cationic distribution takes place when a cation replaces another cation having dissimilar valence state, while maintaining the charge neutrality between Fe^{+2} to Fe^{+3} ions and vice-versa. On doping Cr-Zn in magnetoplumbite structures of Strontium hexaferrites ($SrFe_{12-2x}Cr_xZn_xO_{19}$), Zn^{+2} ions occupy tetrahedral site on replacing Fe^{+3} ions. For charge neutrality Fe^{+2} ions present in octahedral (B) site shift to $Fe^{+3,}$ thereby decreasing Fe^{2+} ionic concentration [77]. Therefore, overall Cr-Zn doping effects in reduction of losses in $SrFe_{12-2x}Cr_xZn_xO_{19}$ system. Zn^{+2} ions have radii equal to 0.74(Å), greater than iron ionic radii. It leads to understand the reason of unit cell volumetric expansion of x= 0.8 and x=1.0 compositions. During analysis, it is also found that porosity is also getting decreased which reveal that densification occurred in the doped samples. Also, unavoidable pores were produced during heating process which caused to decrease measured density.

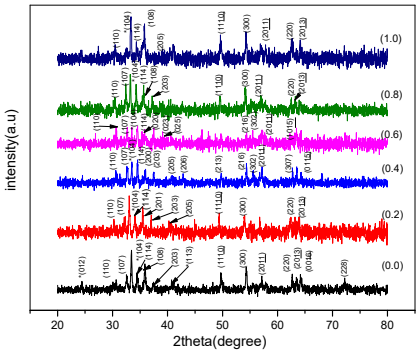

Fig 5.1: XRD patterns of $SrFe_{12-2x}Cr_xZn_xO_{19}$ with composition (x = 0.0, 0.2, 0.4, 0.6, 0.8, 1.0)

Table 5.1: Lattice parameters of Cr-Zn doped $SrFe_{12-2x}Cr_xZn_xO_{19}$ sample series x=0.0, 0.2, 0.4, 0.6, 0.8, 1.0)

$SrFe_{12-2x}Cr_xZn_xO_{19}$	x=0.0	x=0.2	x=0.4	x=0.6	x=0.8	x=1.0
Lattice constant a(Å)	6.0(1)	5.89(3)	5.78(1)	5.78(1)	5.87(1)	5.86(2)
Lattice constant c(Å)	22.99(8)	22.997(8)	22.962(1)	22.98(1)	23.039(3)	23.047(4)
Measured density ρ_m (g/cm^3)	2.36	2.35	2.25	2.61	2.80	3.37
X-ray density ρ_x (g/cm^3)	5.79	4.90	5.35	5.32	5.50	5.75
Porosity (%)	59	52	58	51	49	41
Maximum intensity peak crystallite size $D_{max\ int}$(nm)	67	56	48	42	48	56
Volume of unit cell ($Å)^3$	720.5(9)	692.76(4)	666.43(1)	664.84(1)	687.93(1)	685.58(3)

5.1.2 Lattice Strains

The lattice strains were also calculated by using Williamson-Hall equation which was explained in equation (3.12). Figure 5.2 represent all the plots of $SrFe_{12-2x}Cr_xZn_xO_{19}$ samples for compositions x = 0.0, 0.2, 0.4, 0.6, 0.8, 1.0 respectively. There are two types of strains namely Tensile and Compressional strains. In our Cr-Zn doped magnetoplumbite structure, we observe presence of tensile strains. However, in composition x=1.0, compressional strain was observed. This trend may be produced due to heating effect. Lattice strains (ϵ) values are appended at table 5.2.

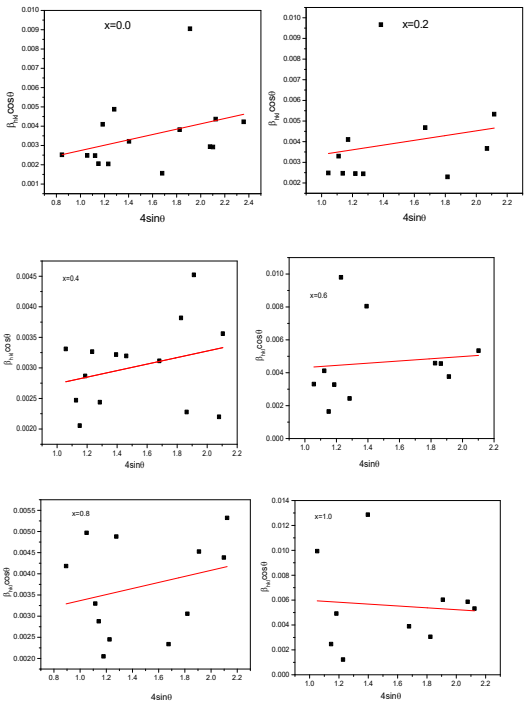

Fig 5.2: Strains plots of $SrFe_{12-2x}Cr_xZn_xO_{19}$ samples for compositions x = 0.0, 0.2, 0.4, 0.6, 0.8, 1.0

Table 5.2: Lattice strains (ϵ) values for sample compositions x = 0.0, 0.2, 0.4, 0.6, 0.8, 1.0.

Composition ($SrFe_{12-2x}Cr_xZn_xO_{19}$)	Strains (ϵ)
X=0.0	0.00139
X=0.2	0.00115
X=0.4	0.00053
X=0.6	0.000673
X=0.8	0.000716
X=1.0	-0.000747

5.1.3 Fourier Transform Infrared Spectroscopy (FTIR) Analysis

Figure 5.3 shows FTIR pattern of Cr-Zn doped magnetoplumbite prepared by co-precipitation method. Magnetoplumbite structure having space group P63/mmc has total 189 optical modes in which 31 modes are infra-red active. The prepared samples showed that all bands lied in the fingerprint ($400cm^{-1}$ to $1400cm^{-1}$) region of Sr-hexaferrites.

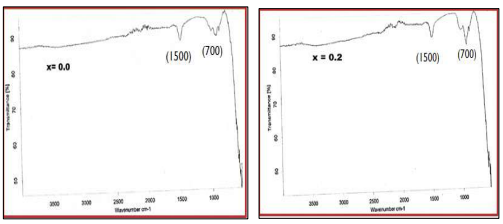

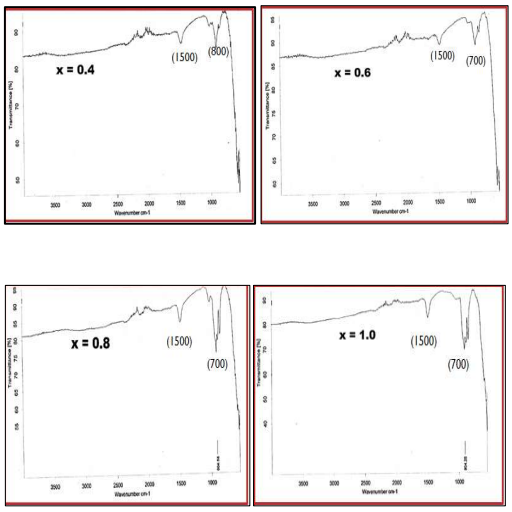

Fig 5.3: FTIR patterns of $SrFe_{12-2x}Cr_xZnxO_{19}$ with composition (x = 0.0, 0.2, 0.4, 0.6, 0.8, 1.0)

5.1.4 Scanning Electron Microscope (SEM) Analysis

Figure 5.4 represents micrographs of $SrFe_{12-2x}Cr_xZn_xO_{19}$ samples powder for all the compositions. Hexagonal structure can be evident for the prepared samples. The particle size estimated for the powdered samples ranged from 8-11µm. Details about the calculated particles size are described in Table 5.3.

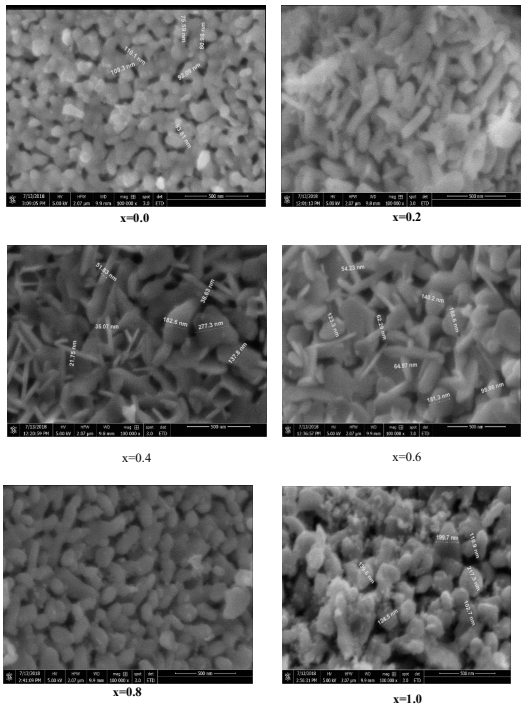

Fig 5.4: SEM micrographs of $SrFe_{12-2x}Cr_xZn_xO_{19}$ samples

Table 5.3: Particle size of powder samples of $SrFe_{12-2x}Cr_xZn_xO_{19}$ samples (x=0.0, 0.2, 0.4, 0.6, 0.8, 1.0)

$SrFe_{12-2x}Cr_xZn_xO_{19}$	x=0.0	x=0.2	x=0.4	x=0.6	x=0.8	x=1.0
Particle size of powder samples (µm)	8	11	8	10	9	11

5.2 AC Electrical Properties with Respect to Frequency and Temperature

5.2.1 Dielectric Constant (ε′)

Polarization can be classified into four types. These are Interfacial or Maxwell-Wagner Dipole, Ionic and Electronic polarization. These polarizations depend on frequency. At lower frequencies, interfacial polarization becomes more active than others and at high frequencies, ionic and electronic polarization become dominant. Dielectric materials are of heterogeneous nature because of the interfaces and high value of resistivity. Such type of nonhomogeneous system can be explained using Maxwell-Wagner model [78, 79]. This response is previously reported about magnetoplumbite ferrites [80].

Figure 5.5 represent dielectric constant (ε') response of all the prepared compositions $SrFe_{12-2x}Cr_xZn_xO_{19}$ synthesized by co-precipitation method. Figure 5.5 shows that as temperature increases, dielectric constant also increases. Such response can be seen for all the prepared sample compositions. Dielectric constant is maximum for sample composition x=1.0 at1 kHz frequency and temperature about 300°C.

The phenomenon of origin of relaxation peaks were also witnessed in prepared samples due to thermal energy imparted to electrons and holes. Thermal energy causes these peaks to shift towards high frequency and temperature regions. The general behavior of ferrites materials is such that dielectric constant is temperature and frequency dependent parameter which is greatly influenced by polarization phenomena. It can be inferred from the plots that when the frequency is increased, the polarization gets reduced and subsequently dielectric constant is also reduced for all the prepared samples.

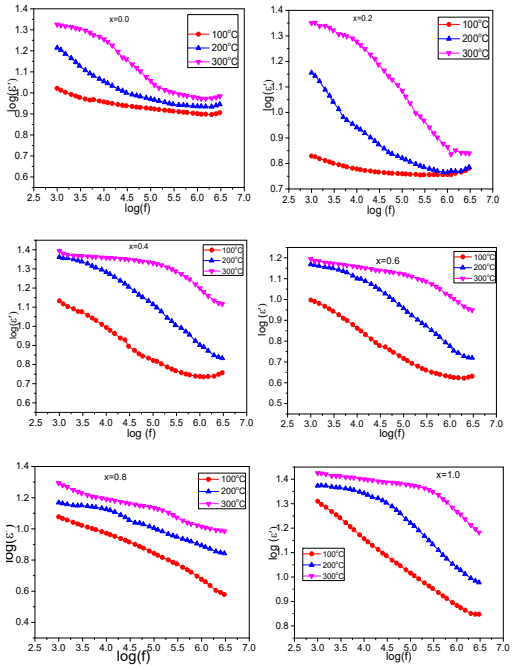

Fig 5.5: Dielectric constant (ε') response with respect to frequency and temperature for $SrFe_{12-2x}Cr_xZn_xO_{19}$ composition (x=0.0. 0.2, 0.4, 0.6, 0.8, 1.0)

5.2.2 Dielectric Loss Tangent (tan δ)

Figure 5.6 represent variation in dielectric loss tangent (tanδ) with changing frequency and temperature for prepared samples of Strontium hexaferrites doped with Cr^{+3}-Zn^{+2}

dopants. The plots in the figure represent that dielectric loss tangent gets decreased as frequency increased. Such behavior can be seen for all the prepared samples. This phenomenon is caused by electrons hopping which takes place between Fe^{+2} and Fe^{+3} sites. When frequency gets increase, electrons hopping could not be successful which resulted in decreased loss tangent. Also, increasing Cr-Zn doping in $SrFe_{12-2x}Cr_xZn_xO_{19}$ system, dielectric loss was observed to be giving increasing and decreasing trend.

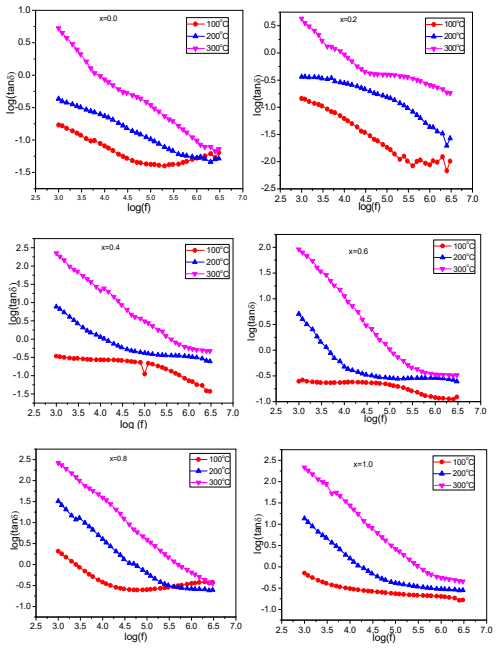

Fig 5.6: Loss tangent (tan δ) response with respect to frequency and temperature for $SrFe_{12-2x}Cr_xZn_xO_{19}$ composition (x=0.0. 0.2, 0.4, 0.6, 0.8, 1.0)

5.2.3 AC conductivity (σ_{AC})

AC conductivity (σ_{AC}) depends upon the successful electrons hopping rate between interstitial sites. From plots of figure 5.7 that AC conductivity increased with increase in frequency and temperature for prepared samples.

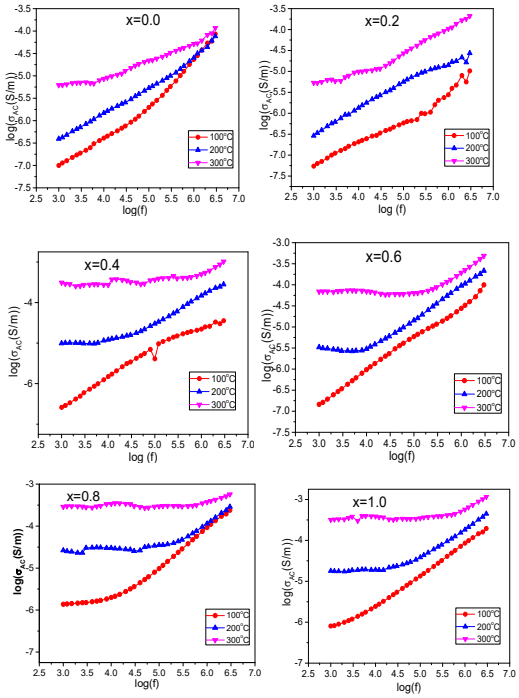

Fig. 5.7: Variations in AC conductivity with respect to Frequency and Temperature

When frequency is low, a plateau region is observed but as soon as frequency and temperature get increased, electron hopping is increased from octahedral (B) to octahedral (B) sites which results in increase of material conductivity. By using relation explained in equation (3.21), the value of 'n' was calculated this value is helpful to define and relate different theoretical model regarding conduction mechanism in the material [81-84]. For example, if 'n' decreases with increase in temperature, it suggests Correlated Barrier Hopping (CBH) model] which is applicable to our system.

In our present study, we calculated the value of 'n' for each sample composition. The plot between $\ln\sigma_{AC}$ and $\ln\omega$ is a straight line, as shown in Figure 5.8. From slope of line, value of exponent can be determined which is found to be range from 0.04-0.8 for the prepared sample compositions, mentioned in table 5.4. This value decreased with increasing temperature, and it may be considered that CBH model is most suitable for our case. Table- 5.4 gives information about the calculated values of n at different temperatures, for prepared samples, as per Jonscher's power law [85].

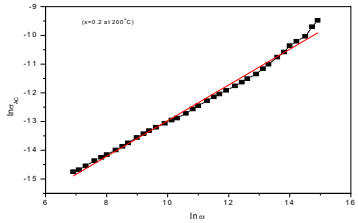

Fig. 5.8: Fitting of plot at 200°C for x=0.2

5.2.4 Impedance (Z)

Electrical properties can be studied by measuring the complex impedance with frequency and temperature. Complex impedance has two parts, one real and imaginary. These parts can be determined by using formula $Z' = z\cos\theta$ and $Z'' = z\sin\theta$ respectively [86-87]. Real part Z' gives material resistance and imaginary part Z'' is related to capacitive nature of material and is given as $Z''=\frac{1}{j\omega C}$ [88].

Table 5.4: Calculated values of 'n' at different temperature for $SrFe_{12-2x}Cr_xZn_xO_{19}$ samples (x=0.0, 0.2, 0.4, 0.6, 0.8, 1.0)

$SrFe_{12-2x}Cr_xZn_xO_{19}$	Temp. 100°C	Temp. 200°C	Temp. 300°C
0.0	0.80	0.62	0.36
0.2	0.58	0.55	0.48
0.4	0.63	0.45	0.11
0.6	0.77	0.59	0.18
0.8	0.69	0.25	0.04
1.0	0.71	0.40	0.10

5.2.4.1 Real Part (Z') of Impedance

Figure 5.9 represents change in the complex impedance real part with changing frequency and temperature. The impedance is found to be decreased for all the sample compositions upon increase with frequency and temperature. Figure 5.9 shows that real part Z' exhibited higher value at low frequency due to all polarizations. Upon increase in temperature, value of Z' experienced a decreasing trend. The graph has two regions as observed and shown in the plot figure 5.9. The first region is the dispersive region and other plateau region. The regions may be originated due to relaxation effects in grain and grain boundaries. Merging behavior of plots can be witnessed in all samples at higher frequencies, irrespective of temperatures. The reason might be space charge polarization effect, observed to be decreased finally, with decrease in barrier potential. This behavior has already been witnessed in Magnetite [89]. Independent plateau region in the plots represent DC resistance. From shape of real impedance curve is function of charge carrier's movement. Curve bears a fall first at temperature about 100°C for sample compositions x=0.0, 0.6, and 1.0. This trend is like AC conductivity graphs obtained for all prepared samples. There is linear increasing and decreasing behavior between the conductivity and resistivity of the materials. Such a behavior in Strontium hexagonal ferrites has already been reported [80].

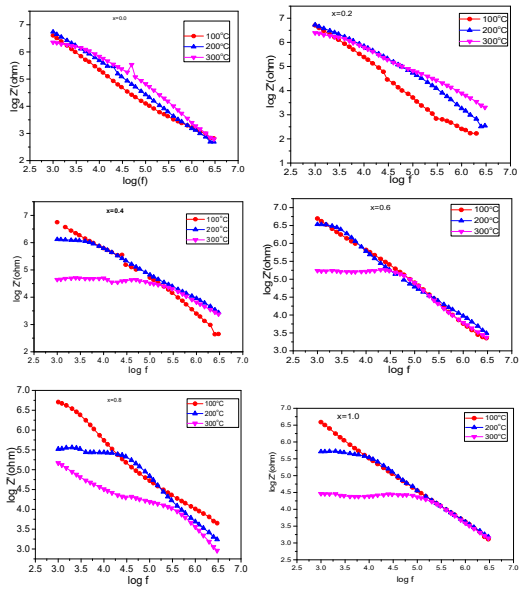

Fig 5.9: Real part of complex impedance with varying frequency and temperature

For long range movements to occur, the successful hoping of charge carriers is a very important factor. The successful hoping of charges takes place due to hopping mechanism during which neighboring charged particles do not move from their positions. As a result, DC conductivity developed, in return, produces DC resistivity, as explained in the impedance plots [90]. Also, unsuccessful hoping of charged particles results into the localized charged movements. The charged carriers stay relaxed about their own position during unsuccessful hoping [90]. It helps in generation of AC conductivity and causes origination of dispersive regions as shown in the plot [91-92]. Grain and grain boundaries effects are found in inhomogeneous materials.

Based on conduction phenomenon, extrinsic and intrinsic behavior can be explained [92].

5.2.4.2 Imaginary part (Z″) of Impedance

Figure 5.10 explains the changes in imaginary part (Z″) of the impedance with changing frequency and temperature. Plot shows on increasing frequency and temperature parameters, imaginary part (Z″) starts to decrease. The trend is seen in plots of all the compositions. At a characteristic or relaxation frequency, it is observed that relaxation peaks are produced for samples x=0.6 and x=0.8. These peaks seem to be shift towards high frequency regions.

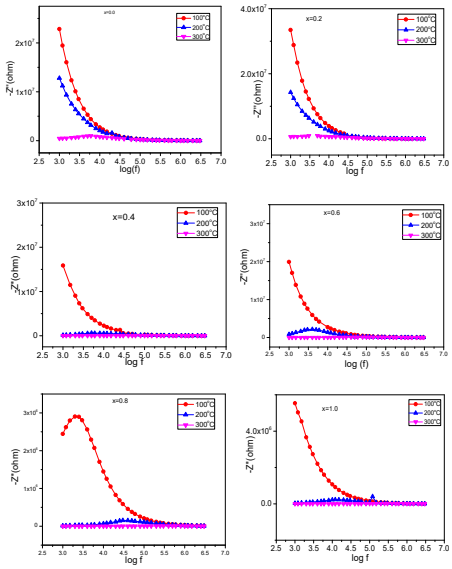

Fig. 5.10: Imaginary part of complex impedance with respect to frequency and temperature

5.2.5 Cole-Cole Plots

To understand conduction processes, Nyquist or Cole-Cole plots have been drawn between imaginary parts Z″(w) and real parts Z′(w) of complex impedance for prepared sample compositions of $SrFe_{12-2x}Cr_xZn_xO_{19}$ (x=0.0, 0.2, 0.4, 0.6, 0.8, 1.0) at different temperatures. Figure 5.11(a) is relevant. Generation of arcs and semicircles features can be witnessed in the figure. These features are formed due to diverse relaxation behavior. These arc features can be helpful to explain the Conduction mechanism. It is observed that unsymmetrical and semicircle arcs are produced about 100°C, in all the prepared sample compositions. It suggests non-Debye type relaxation in prepared hexagonal ferrites [90].

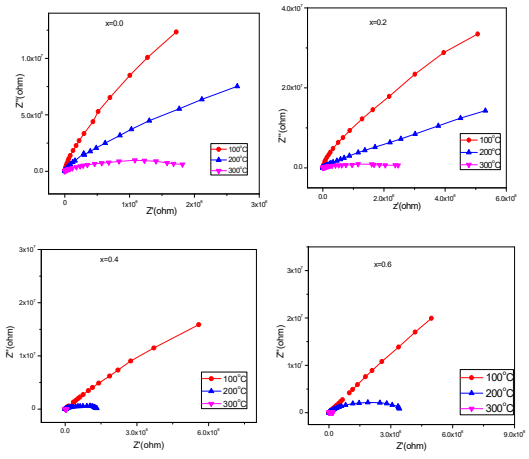

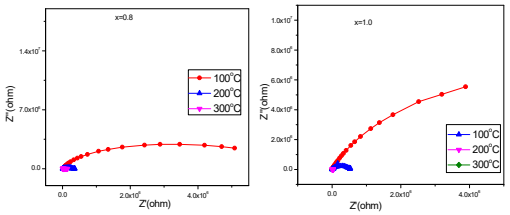

Fig 5 .11 (a): Variation between $Z''(w)$ and $Z'(w)$ for the different compositions at different temperatures

In Cole-Cole plots, intercepts of semicircle on real axis (Z') is often helpful in determining materials bulk resistance (Rb). Cole-Cole plot shows that diameter of semicircles decreases and gradually shifts to origin upon increase in temperature. Such type of decrease in material's Rb is already reported in literature [93]. With increasing temperature, arc radius also starts decreasing. It indicates the material's semiconducting nature. Also, we assume that large semicircle arcs are responsible for grain boundary effect at room temperature. It means that as temperature rises, generation and accumulation of charge carriers gets start across different interfacial discontinuities [94]. Every arc represents specific nature of relaxation process [95]. Their radii measure materials resistances produced in different regions [96].

In a case when a perfect semicircle is observed with center at abscissa, is an indication of Debye-type conduction process. Figure 5.11(b) explains details plots at about 300°C temperature for the entire prepared sample. To explain the electrical behavior of prepared samples, Z-view software has been used. To understand material at microscopic level, RC circuits were obtained. For instance, fitted model (RQ) (RC) can be proposed for x=0.4. For compositions (x= 0.0, 0.2, 0.6, 0.8, 1.0) fitted model were (RQ)(RQ), here R defines the resistance, C capacitance and Q the Constant Phase Element (CPE). Q element can be used for tuning non-ideal capacitive behavior in circuits [97].

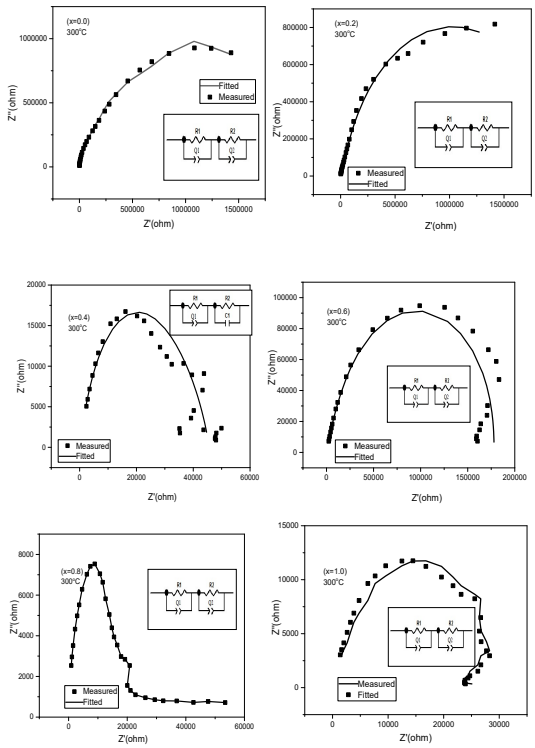

Fig 5.11(b): The Cole-Cole for the prepared samples at temperature 300°C

Table 5.5 describes all the values determined after fitting parameters at about 300°C temperature. The grain boundary effect can be seen dominant at 300°C for all the sample compositions.

Table 5.5: Fitting parameters for $SrFe_{12-2x}Cr_xZn_xO_{19}$

Different Parameters	$SrFe_{12-2x}Cr_xZn_xO_{19}$					
	x=0.0	**x=0.2**	**x=0.4**	**x=0.6**	**x=0.8**	**x=1.0**
R1 (Ω)	164790	$2.022x10^{6}$	29195	43027	19327	4984
R2 (Ω)	$2.0x10^{6}$	16785	16483	135040	29321	21231
Q1	$2.282x10^{-11}$	$6.289x10^{-11}$	$1.834x10^{-9}$	$4.614x10^{-10}$	$2.06x10^{-10}$	$1.040x10^{-9}$
Q2	$2.639\ x10^{-11}$	$9.791x10^{-12}$	-	$3.765x10^{-12}$	$1.0x10^{-20}$	$2.444x10^{-11}$
C1(F)	-	-	$2.542x10^{-11}$	-	-	-
τ(s)	$2.40\ x10^{-6}$	$2.60\ x10^{-5}$	$8.58x10^{-7}$	$6.91x10^{-7}$	$5.10x10^{-7}$	$1.51x10^{-7}$

5.3 Electrical Properties at Fixed Frequencies of 500 kHz and 1- MHz

5.3.1 Dielectric constant (ε')

Figure 5.12 represents dielectric constant response varying with temperature from 100°C to 500°C at fixed frequencies of 500 kHz and 1-MHz. The change in the dielectric response is such that it increases with increase in temperature at both frequencies for all the prepared samples. However, value of dielectric constant is observed to be higher at 500 kHz than the value at 1-MHz. This may be due to the reason that the thermal energy in the system increased the process of polarization because the frequencies were fixed, and the leading role was played by temperature. The hopping between Fe^{+2} and Fe^{+3} ions enhance the polarization process at octahedral (B) site. The response of dielectric constant plots displays that in the start, its value increases with temperature and then a decrease in its value can also be seen. This decreased response may be caused due to saturation of charge carriers [98]. The dielectric constant decreases about temperature 400°C - 500°C, called transition temperature T_d. This is the temperature at which material transforms to paraelectric nature from ferroelectric. This behavior has already been reported on magnetoplumbite hexagonal structures for Pb^{+2} doped Strontium hexaferrite material [99]. The reason for

the decrease in the value of dielectric constant response at 1-MHz frequency might be due to effect of multi-particle polarization.

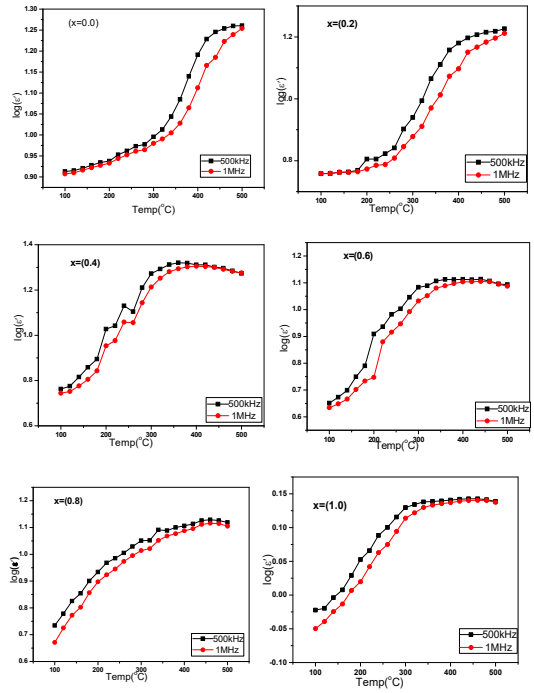

Fig 5.12: Dielectric constant response with temperature at fixed frequencies 500 kHz and 1-MHz for $SrFe_{12-2x}Cr_xZn_xO_{19}$ samples (x-0.0, 0.2, 0.4, 0.6, 0.8, and 1.0)

5.3.2 Dielectric Loss Tangent (tan δ)

Figure 5.13 represents the change in loss tangent (tan δ) response with varying temperature from 100°C to 500°C for fixed frequencies 500 kHz and 1-MHz. It can be seen from the plot that there is an increasing trend in loss tangent for all the samples however, it is higher at 500 kHz frequency than at 1-MHz. In case when frequency is low and temperature is also low, dipoles align themselves in the same direction as that of the applied field direction. With the increase in temperature, temperature forces dipoles to orientate themselves by rotational or orientation motion. The resultant effect is an increase in the loss tangent. When the frequency is increased up to 1-MHz, the rate of successful hopping between octahedral (B) site to octahedral (B) sites is decreased due to which charge carriers do not withstand the field effects. The polarization was decreased and subsequently, tan loss also decreases [100]. Loss tangent can be defined as the dissipated heat energy, for which system is unable to use that. The heat dissipated depends on electron, generated in a result of thermal effects. Value of loss tangent is observed to be lowest at about 1-MHz frequency in all prepared samples. This certain behavior has already been witnessed in Strontium hexaferrites and was also reported [101].